NARSIS

New Approach to Reactor Safety ImprovementS

WP2: Fragility assessment of main NPPs critical elements

D2.3 - PhD narrative on the seismic structural response of corroded RC components

Project Acronym: NARSIS

Project Title: New Approach to Reactor Safety Improvements

Deliverable: D2.3 - PhD narrative on the seismic structural response of corroded RC components

Month due: 44   **Month delivered:**   55

Leading Partner: CEA

Version: Final

Primary Author: Chaymaa LEJOUAD (EDF)

Other contributors:

  - CEA: Philippe MONGABURE

Deliverable Review:

  - **Reviewer:**   E. FOERSTER (CEA)

Dissemination Level		
PU	Public	**X**
PP	Restricted to other programme participants (including the Commission Services)	
RE	Restricted to a group specified by the consortium (including the Commission Services)	
CO	Confidential, only for members of the consortium (including the Commission Services)	

Table of contents

List of Figures

List of Tables

1   Executive Summary

The present document aims at providing an extended summary of the main PhD works related to the NARSIS WP2, task2.2.1. These works were performed by Chaymaa Lejouad, formerly PhD at CEA Paris-Saclay, under the supervision of Dr. Benjamin Richard (IRSN), Profs. Frédéric Ragueneau & Sophie Capdevielle (Ecole Normale Supérieure Paris-Saclay) and M. Philippe Mongabure (CEA Paris-Saclay).

The full Ph.D. manuscript (Lejouad, 2020, in French) is publicly available at the following link:

https://tel.archives-ouvertes.fr/tel-03130591

The reported works were focused on the experimental and numerical assessment of corrosion pathologies, which may lead to a loss of structural performance of reinforced concrete (RC) members under seismic loadings (Lejouad et al., 2019a,b; Lejouad et al., 2022a,b).

For this purpose, a long-run experimental campaign was conducted on the AZALEE shaking table and the strong floor belonging to the TAMARIS seismic experimental facility operated by CEA Paris-Saclay. Three configurations of steel rebars and three corrosion rates were considered in the analysis, with the corrosion being imposed to the RC specimens in a short time frame, thanks to the use of an accelerated corrosion technique (imposed current). Quasi-static cyclic and dynamic testing of corroded large-scale RC beam specimens were performed, in order to quantify some quantities of interest: ductility ratios, evolution of eigenfrequencies and damping ratios, as a function of the corrosion rate. The observed trends w.r.t the modal characterizations showed that the modal properties are not reliable damage indicators.

Regarding the numerical aspects, a corrosion model for the rebars has been developed to be used in finite-element computing codes, in order to simulate the seismic behaviour of corroded RC structures. The modelling strategy to account for corrosion effects, is based on Timoshenko fibre beam elements (Pegon, 1994; Guedes et al., 1994), these elements being quite efficient when carrying out computations at a structural scale. This numerical model is able to account for the following damaging mechanisms (corrosion effects):

- Initial concrete damage due to the expansive nature of the corrosion products;
- Random distribution of the diameters along the rebars to account for corrosion pits;
- Mechanical strength reduction of the corroded rebars.

In the proposed strategy, the damage distribution due to corrosion is first computed as an initial material state, in the beam cross-section, using a fine mesh. Then, a coarser mesh is used, to save time in the dynamic computations used to assess the overall structural response. This is done by using a field projection method, which allows to minimise the difference between the two cross-section (initial and projected) stiffness matrices. The steel mechanical degradation is then taken into account through the constitutive model while the spatial distribution function for the corrosion pits is determined from the experimental measures performed on the corroded rebars sections. The proposed numerical model is thus capable of predicting the beam failure in agreement with the experimental results. In addition, it has been shown that taking cracking into account improves the prediction of the structural responses at low loading levels for the most corroded beam. However, the determination of the expansion coefficient to be considered in the simulations remains a difficult task.

In conclusion, this work has improved the state of knowledge on the dynamic behaviour of weakly corroded structural elements (3% to 9% loss of mass), as well as on the most determining elements to be considered in the numerical simulations and models, in order to predict the seismic response of corroded structures.

2 Introduction

The European H2020 research project NARSIS focuses on the development of methodologies for Probabilistic Safety Assessment (PSA) of Nuclear Power Plants (NPPs) against external natural hazards.

Corrosion of steel reinforcement being one of the most widespread pathologies leading to a loss of structural performance of Reinforced-Concrete (RC) members, it is crucial to characterize and understand this pathology, especially when it is combined with earthquakes.

The main objective of the PhD works reported hereafter, was to experimentally assess the influence of the steel rebar corrosion on the quasi-static cyclic and dynamic responses of RC elements and structures. In the section 3, we summarize the long-run experimental campaign conducted on large-scale RC beams, using the AZALEE shaking table and the strong floor belonging to the TAMARIS seismic experimental facility operated by CEA Paris-Saclay.

A second objective, presented in the section 4, was to propose a modelling strategy based on the finite-element approach, in order to account for corrosion effects, when simulating the seismic behaviour of existing RC structures.

3   Experimental campaign and main results

3.1   *Introduction*

Reinforced concrete (RC) is commonly used for buildings as well as for nuclear facilities, due to its low cost, good mechanical properties and satisfactory durability properties. However, the service-life of RC structures may be reduced along time with the emergence of pathologies, such as the steel reinforcement corrosion which leads to a decrease of the structural performance of RC members.

In the nuclear industry, the steel reinforcement corrosion might potentially be a concern, especially for the Nuclear Power Plants (NPP), e.g., located in a coastal environment. For this reason, nuclear operators are required to carry out maintenance operations throughout the structure lifetime. Based on some periodical structural auscultations, these operations seek to restore the initial structure bearing capacity without considering the dynamic response, less studied in the case of corrosion pathology.

Therefore, the experimental works performed in this PhD (Lejouad et al., 2019a,b; Lejouad et al., 2022a,b) aimed at understanding the mechanical consequences of steel reinforcement corrosion on both quasi-static and dynamic behaviours of RC structural members.

3.2   *Presentation of the experimental campaign*

3.2.1   *Tested RC specimens*

The experimental campaign, named DYSBAC, was performed by means of the AZALEE shaking table and the strong floor, which are parts of the TAMARIS experimental facility operated by CEA on the Paris-Saclay site. The main objective of this campaign was to study the influence of corrosion on the seismic behaviour of some corroded RC members, considering various loading conditions, i.e., quasi-static cyclic loadings on the strong floor and dynamic loadings on the shaking table. Allowing to these various loading conditions, different analyses were to be performed: study of the bearing capacity, energy dissipation, hysteretic capacity, evolution of the natural frequencies, loading amplification, mode shapes, etc.

The choice of large-scale RC beams was made, considering some design constraints, e.g., related to the size of the testing strong floor (4.5 m length), the maximal stroke of the available actuator (± 400 mm) and the operating frequency range of AZALEE shaking table (0.1-30 Hz). The beams were cast with a low strength concrete, representative of the concrete in existing RC structures. The concrete had a compressive strength equal to 30 MPa.

The steel reinforcement was designed according to the European standards (Eurocodes 2 and 8). It can be classified as B500A, according to the French steel classification, with an average yield strength equal to 500 MPa and an ultimate strain equal to 2.5%.

The final design is shown on Figure 1.
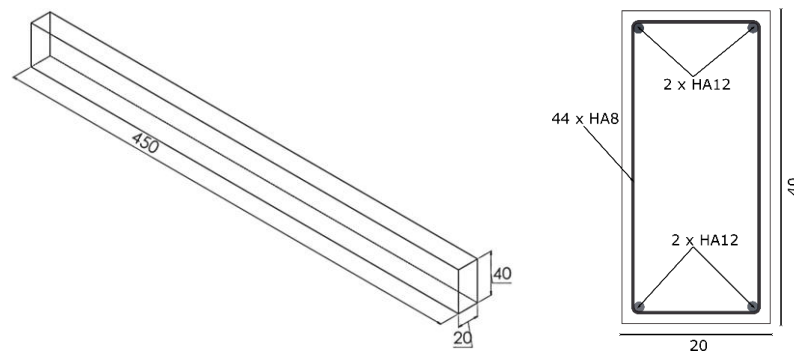
Figure 1. RC beam design (sizes in cm): geometry (left) and reinforcement details (right)

3.2.2   Corrosion procedure

In order to study the effects of corrosion of each reinforcement part, three beam corrosion configurations were: C_1 for longitudinal reinforcement corrosion, C_2 for transverse reinforcement corrosion and C_3 for the complete reinforcement corrosion.

Since a natural corrosion process is highly time-demanding and hence, cannot be envisaged during a PhD time frame, an accelerated corrosion technique by imposed current was used. It consists in applying an electrical current from a DC power supply (Direct Current) between the cathode (stainless steel grid) and the anode, i.e., the RC specimen reinforcement. The whole specimen is immersed in an electrolytic solution containing chlorides to guarantee electrical conduction and to be representative of the corrosion process by chlorides. Figure 2 shows a simplified representation of the setup for accelerated corrosion by imposed current, as well as a top view of the experimental campaign's beams subjected to the accelerated corrosion technique through immersion in a 3.5% NaCl solution.

Figure 2. Accelerated corrosion technique: set-up principle (left) and CEA beams under corrosion (right).

25 beams were cast on site: 8 for configuration C_1, 8 for C_2 and 9 for C_3. For each configuration, a non-corroded (NC) beam was kept for reference.

Hereafter, the main aspects of each corrosion configuration are recalled:

C_1 beam configuration: corrosion of longitudinal bars only

The stirrups were insulated so as to have only the longitudinal bars crossed by the electrical current. Each longitudinal bar was considered as an anode with an independent cathode in stainless steel (Figure 3a).

C_2 beam configuration: corrosion of stirrups only

The insulation was put on the longitudinal bars at the connection points with the stirrups, thus only stirrups were crossed by the electrical current. The full beam was wrapped with the stainless-steel grid (Figure 3b).

C_3 beam configuration: full corrosion

No insulation was put: the reinforcement (longitudinal bars and stirrups) was crossed by the electrical current. The full beam was also wrapped with the stainless-steel grid (Figure 3b).

(a)   (b)
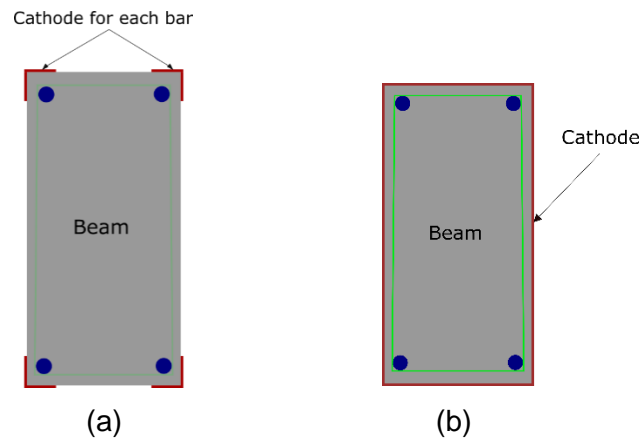
Figure 3. Cathode position: (a) C_1 configuration (b) C_2 and C_3 configurations.

The current density was limited to 100 µA/cm² in order to be more representative of natural corrosion (Caré & Raharinaivo, 2007). Three corrosion rates expressed in terms of mass loss were targeted:

- 5%: threshold for the bond loss between steel and concrete (Auyeung et al., 2000);
- 10%: rate from which civil engineering maintenance operations begin (Cremona, 2009);
- 15%: it is believed to be the threshold from which a change of failure mode is observed (Almusallam, 2001; Meda et al., 2014; Ouglova, 2004).

For each type of beam, the exposure duration and corrosion rates were estimated using the Faraday's law:

$$\Delta t = \frac{\alpha \, . \, \Delta w \, . \, z . F}{M . I} \tag{1}$$

With:

Δw Steel mass consumed due to corrosion (kg.m^{-2})
I Current density (A.m^{-2})
Δt Exposure time (s)
F Faraday constant (96,500 A.s^{-1})
z Ionic charge (2 for Fe)
M Atomic weight of metal (g.mol^{-1})
α Coefficient usually taken between 1 and 2, to account for the duration of chloride ingress into concrete before reaching the rebar ($\alpha = 1.3$ in this study).

Table 1 sums up the estimated exposure time for each corrosion degree and each beam configuration.

Table 1: Beam exposure durations (in days) for the various corrosion configurations

Corrosion rate (%)	Exposure durations (days)		
	C_1 (all HA12 bars)	C_2 (44 HA8 stirrups)	C_3 (4 HA12 bars & 44 HA8 stirrups)
5	47	31	36
10	94	62	72
15	141	94	109

3.2.3   Seismic testing of the corroded RC beams

The experimental campaign included quasi-static (QS) cyclic as well as dynamic (DYN) testing. The setup was similar to the one used in the campaign conducted by Heitz et al. (2018), but adapted for high-range displacements and rotations. The beams were excited along their weakest flexural axis, applying the following boundary conditions:

- spinning supports allowing rotation at beam ends;
- two air-cushion systems to bear the beam weight and to drastically reduce the friction between the beam and the shaking table's or strong floor's upper plate.

Instrumentation setup

The same instrumentation was used for quasi-static and dynamic tests (Figure 4). The various sensors used to fully characterize the beams mechanical response during the tests, were the following:

- 5 wired displacement sensors;
- 2 high-precision displacement sensors;
- 2 force cells (6 axes);
- 7 accelerometers (3 axes).
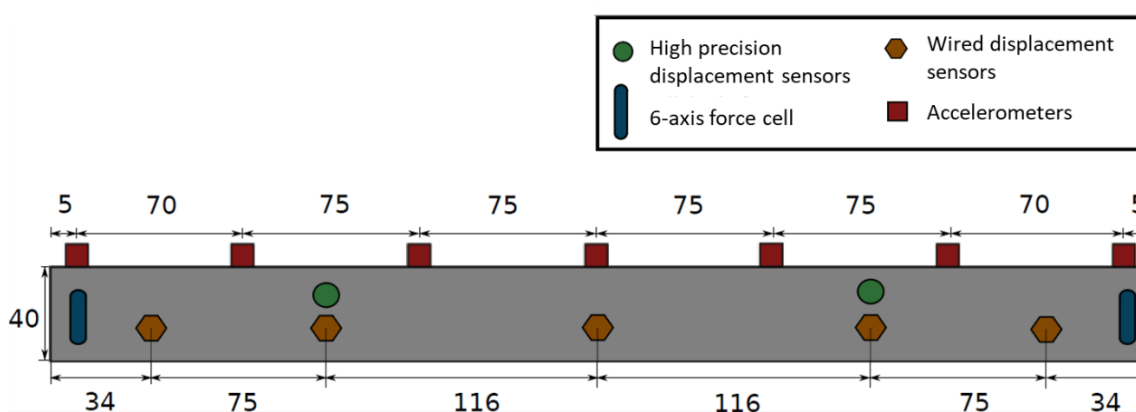
Figure 4. Instrumentation used for quasi-static and dynamic tests

A digital image correlation technique was also used during the quasi-static and dynamic tests (Figure 5). This technique consists in following the displacement of a painted strip on the upper surface of the beam, using a stereoscopic video system fixed on a crane above testing area. Images are then used to compute the shape of the beam during the tests.
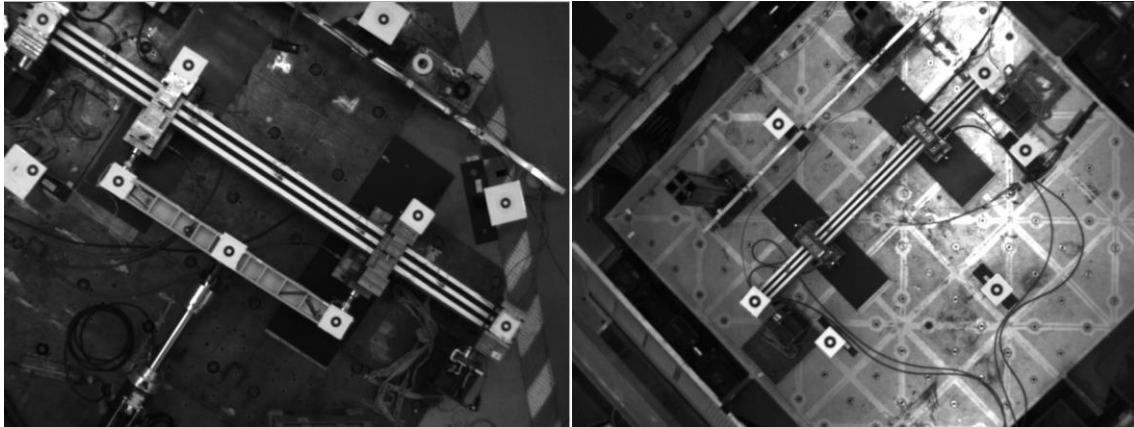
Figure 5. Stereoscopic views for image correlation: quasi-static tests (left); dynamic tests (right)

a) <u>**QS cyclic tests**</u>

During the QS testing, the corroded and NC beams were subjected to standard 4-point alternate bending tests performed on the TAMARIS strong floor, using a long-stroke hydraulic actuator (100 kN, ±500 mm) to apply the loading. The experimental setup is shown in Figure 6.
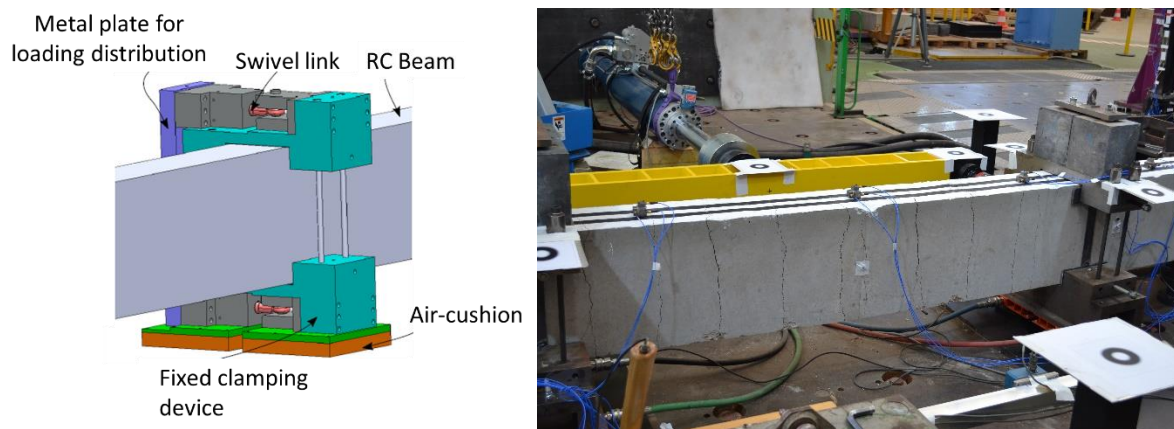
Figure 6. Intermediate beam supports (left) and strong floor experimental setup (right) used for quasi-static tests

The loading included blocks of 3 identical cycles of prescribed displacements, with an increasing amplitude between two consecutive blocks (Figure 7) and a loading velocity kept constant (0.5 mm.s^{-1}). The amplitude range was between 0.4 and 200 mm. Each cycle involved 4 phases: loading in one direction, unloading, loading in the other direction and unloading.

The objective of having 3 cycles was to stabilize the damage levels within the current block before moving on to the next one. Indeed, during the 1st block cycle, the damage level increases due to cracking, while energy dissipates during the remaining two cycles, due to the cracks work. The aim of the QS testing was hence to assess the evolution of the hysteretic energy dissipation quantified for the last 2 cycles.

In addition, each tested specimen was subjected to hammer shock tests, performed between the different loading blocks, in order to quantify the evolution of the modal properties (natural frequencies, mode shapes) with increasing damage and as a function of the corrosion rate and the corrosion configuration.
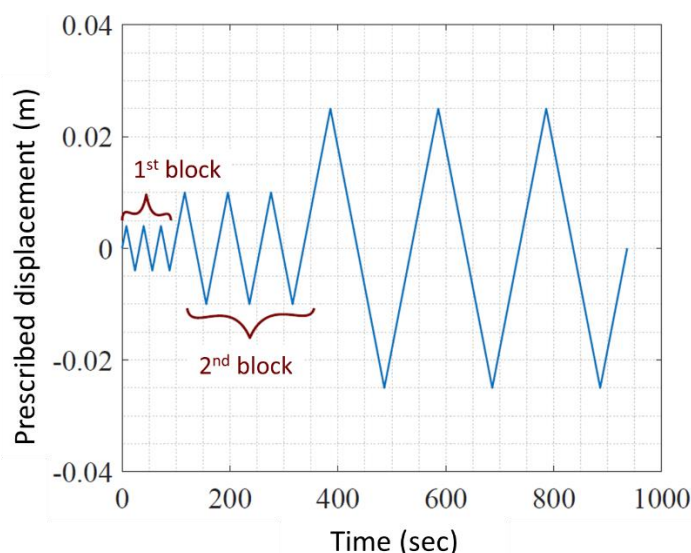
Figure 7. Cyclic loading applied for the quasi-static tests

b) Dynamic tests

The DYN tests were used to quantify the evolution of the modal properties, hence enabling to fully characterize the mechanical state due to corrosion. They were performed on AZALEE, a 6 x 6 m² shaking table with 8 hydraulic actuators (6 degrees of freedom: 3 rotations, 3 translations), 100 tons payload and capable of reproducing seismic signals up to 5 g. Two additional masses (310 Kg each) were fixed at the intermediate supports bringing the first natural frequency of the beams close to 12 Hz. The dynamic experimental set-up is shown on Figure 8.
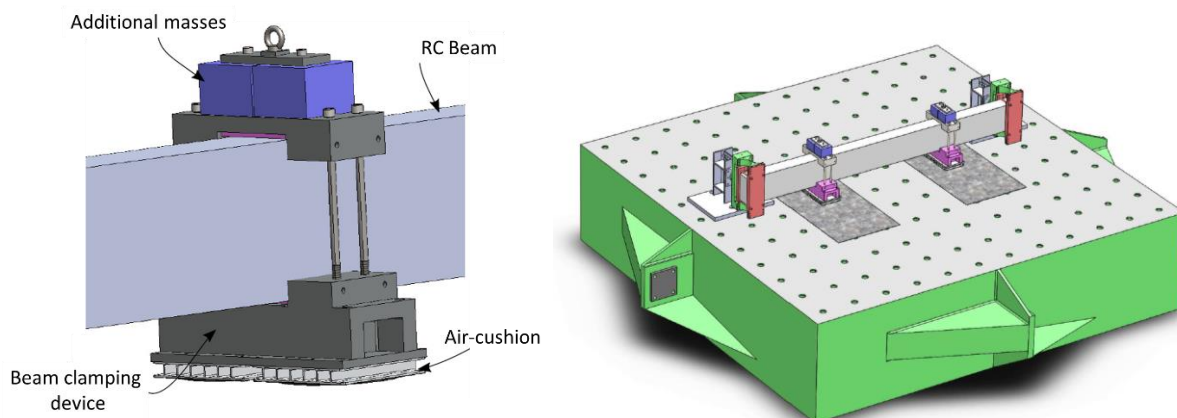
Figure 8. Intermediate beam supports (left) & shaking table experimental setup (right) used for the dynamic tests

The dynamic loading consisted in a synthetic signal able to excite only the first natural mode of the beam (Figure 9). The signal bandwidth was between 1 and 13 Hz, in order to anticipate the modal frequency drop due to damage and to allow to constantly excite the sought modal frequency all along the test. Five acceleration levels were tested, namely considering: 0.125 g, 0.5 g, 0.8 g, 1.25 g and 2 g (see example in Figure 10). A modal characterization of each beam was performed using a white noise signal (0.07 g), before testing and in-between consecutive testing sequences.
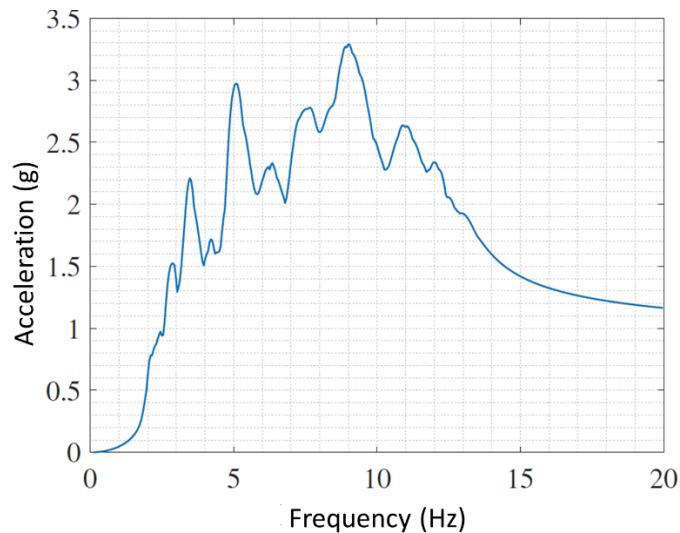
Figure 9. Response spectrum of the synthetic excitations used for the dynamic tests
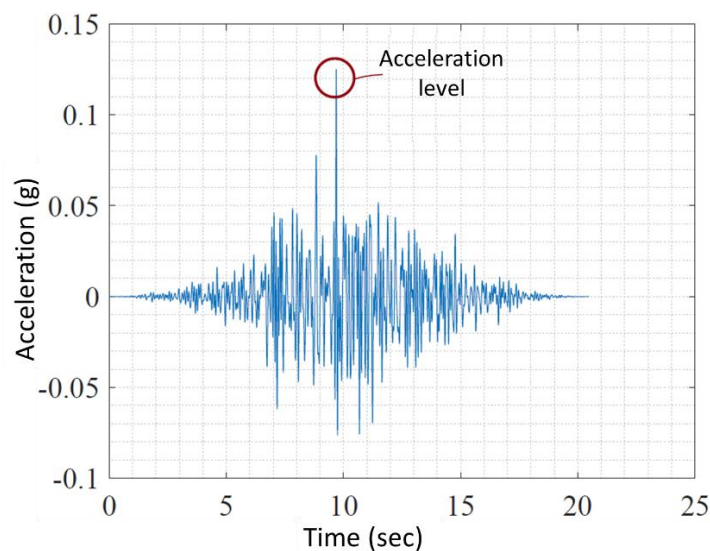
Figure 10. Example of a synthetic excitation generated for the dynamic tests and corresponding to an acceleration level of 0.125 g

3.3 Main experimental observations

The experimental observations for the QS cyclic tests were the following:

- All beams reached total failure, due to the yielding of the steel rebar (bending mode).
- C_2 and NC beams exhibited similar imposed and maximum (at failure) displacements at mid-span, whereas these displacements were reduced for C_1 and C_3 beams.

The failure of the longitudinal rebar did not occur systematically at mid-span, but rather depended on the corrosion pit distribution.

Figure 11 depicts the failure modes observed for some NC and C_1 beams at the end of the QS loadings.
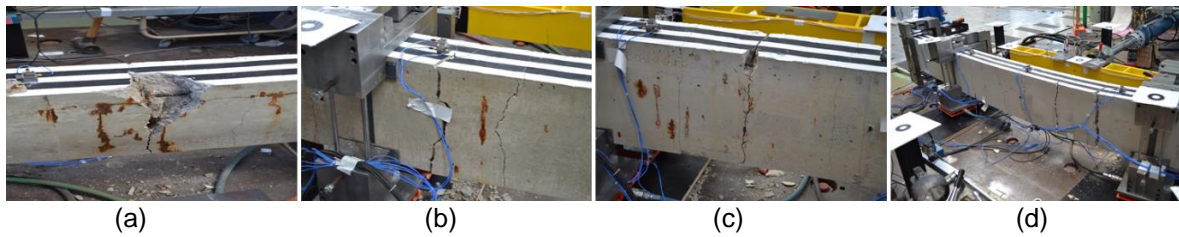
Figure 11. Failure modes for some beams under QS cyclic loading: NC (a) and C_1: 5% (b), 10% (c), 15% (d)

The experimental observations at the end of the DYN tests were the following:

- Only the beams in the configurations C_1 with 10% and 15% corrosion rates, as well as C_3 with 5% and 10% corrosion rates, did reach failure (bending mode as for QS tests). Allowing to the configuration, the failure was not systematically observed at mid-span.
- The NC and other corroded beams exhibited bending cracks at the concrete level, with a yielding of reinforcement rebars, and plastic hinges appearing at mid-span.

Figure 12 depicts the failure modes of some corroded beams at the end of the DYN loadings. It shows that allowing to the configuration, the failure was not observed systematically at mid-span (e.g., Figure 12b).
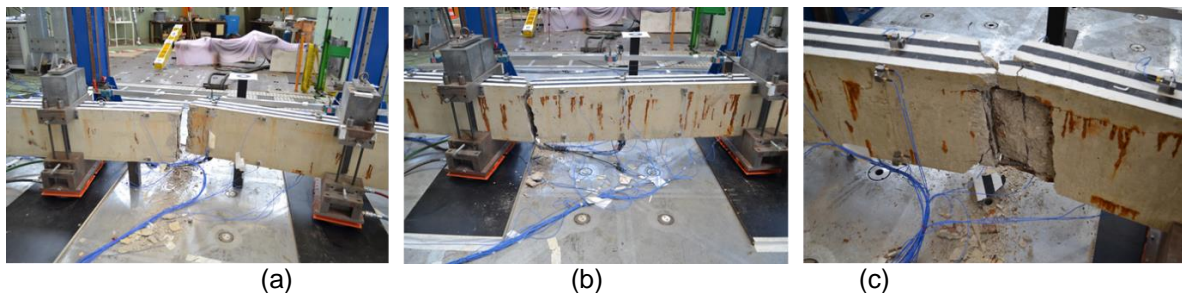
Figure 12. Failure modes for some beams under dynamic loading: C_3 5% (a), 10% (b) and C_1 15% (c)

3.4 Analysis of the structural response

3.4.1 Main results for the QS cyclic tests

The structural responses of the NC and corroded beams in each corrosion configuration are compared on Figure 13: the maximum displacement measured at mid-span was similar for all beams until 25 mm of imposed displacement. Beyond this value, displacements for the corroded beams were slightly higher than those of the NC beam. The same trend was observed in some former studies (Yuan et al., 2018).
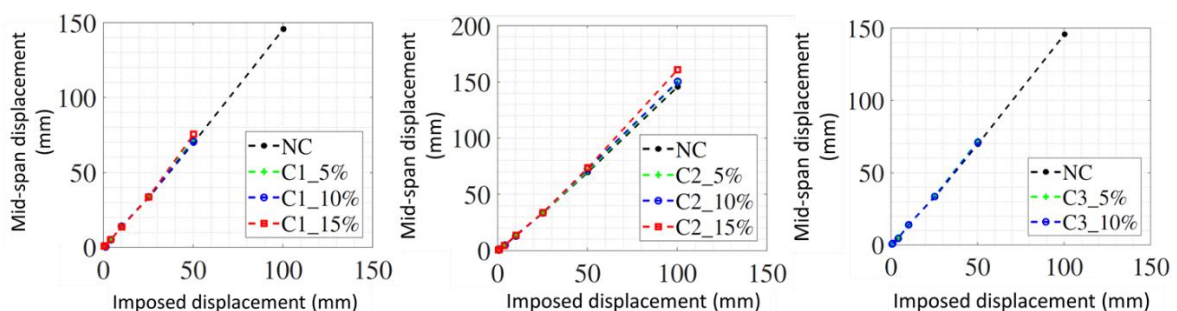
Figure 13. Measured displacements for all beam configurations under QS cyclic loading

3.4.2 Main results for the dynamic tests

As in the section 3.4.1, the same trends were observed on measured displacements with respect to the PGA (Peak Ground Acceleration) (Figure 14): similar mid-span displacements for all beams until 0.5 g and then a slight increase for the corroded beams, compared to the NC beams. As for the measured mid-span accelerations (Figure 15), the response of the C_1 (10 & 15%) and C_3 (5 & 10%) beams was globally lower than for the NC beam. In this study, the amplification factor, i.e. the ratio between the measured mid-span acceleration peak and the PGA measured on the shaking table, varied between 1.6 and 5.
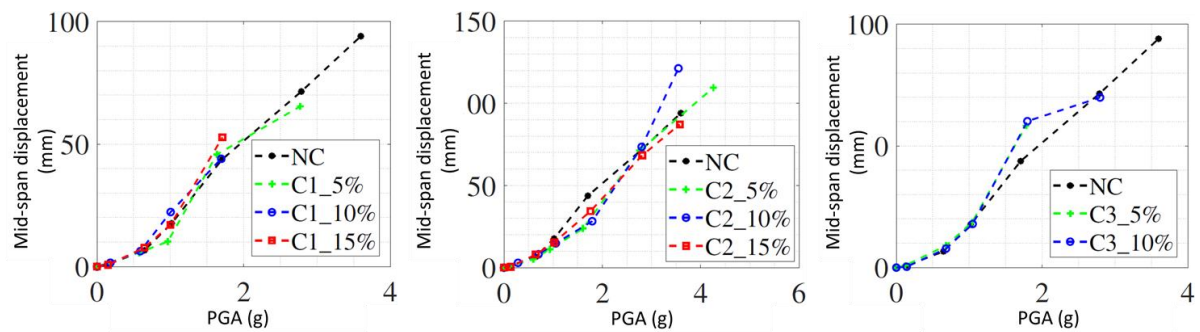
Figure 14. Measured displacements for all beam configurations under DYN loading
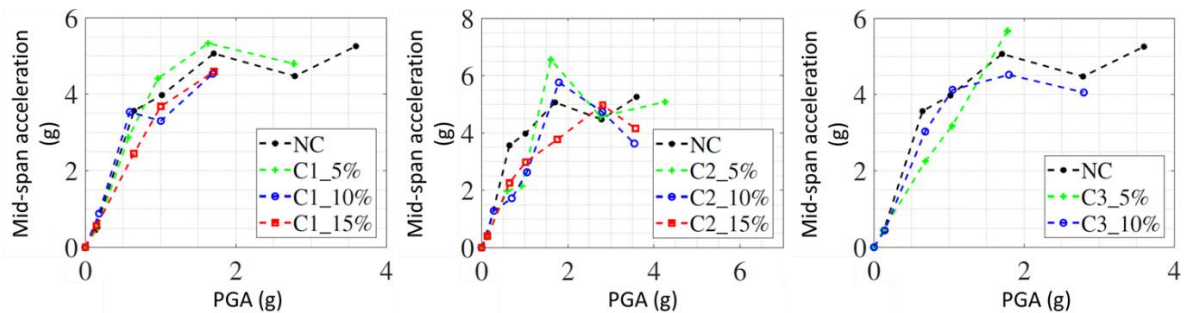
Figure 15. Measured accelerations for all beam configurations under DYN loading

3.5 Analysis of the Hysteretic response

3.5.1 Main results for the QS cyclic tests

The nonlinear behaviour of RC elements under cyclic loadings can be expressed by plotting the force vs. displacement curves (e.g., Figure 16), where the energy dissipation during the cyclic loading can be quantified via the areas of the obtained hysteretic loops. This dissipation feature is crucial for the anti-seismic design, as it helps limiting potential structural damages by reducing the amplitude of the oscillations produced during the seismic loading.

The curves in Figure 16 depict the force obtained by summing the support reactions measured along the applied loading direction for both ends of the tested beam. The displacements were measured at beam mid-spans. Only tests preceding failure are shown in this figure. We note that the higher the corrosion rate, the higher the decrease in dissipated energy accumulated for each configuration during the testing sequences. This result has been also observed by other authors (e.g., Ma et al., 2012; Guo et al., 2015).
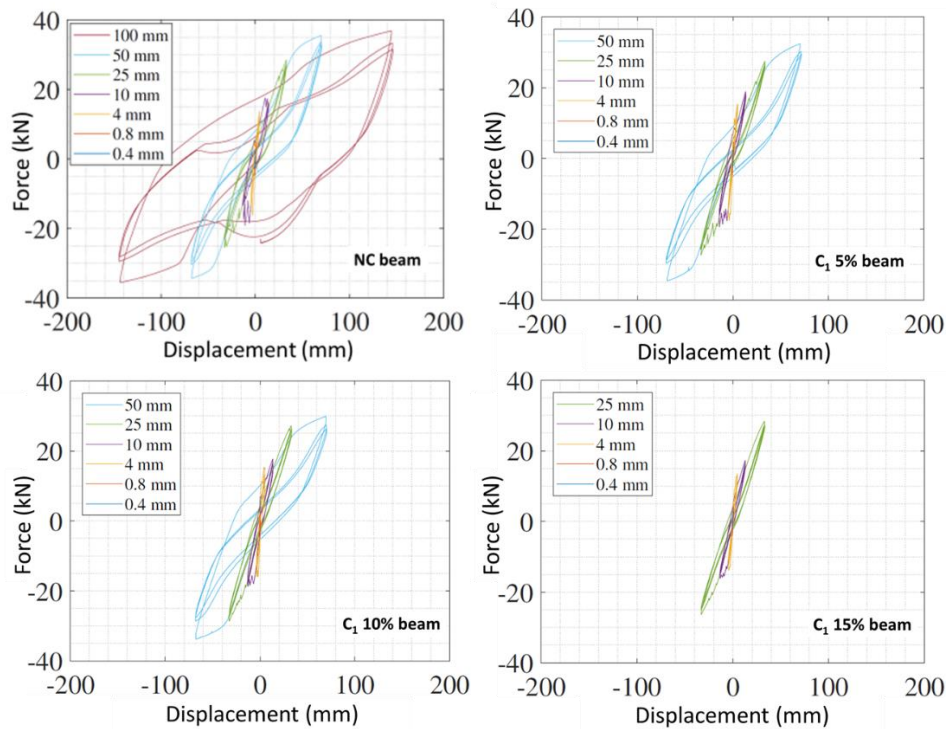
Figure 16. Hysteretic experimental response of some corroded beams under QS cyclic loading

3.5.2   *Main results for the dynamic tests*

The same hysteretic behaviour trend was obtained, as shown on the force-displacement curves of the NC and C_1 configurations in Figure 17: the accumulated energy dissipation decreased when the corrosion rate increased.
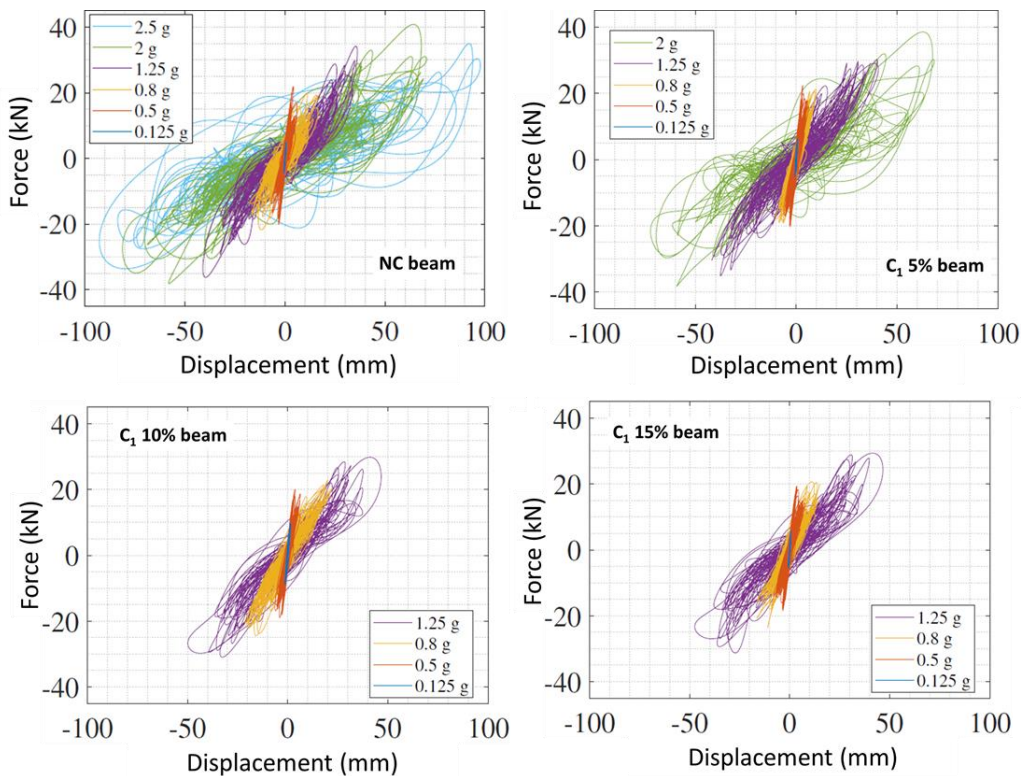
Figure 17. Hysteretic experimental response of some corroded beams under DYN loading

3.6 Analysis of the capacity curves and ductility

3.6.1 Main results for the QS cyclic tests

In Figure 18, we plot the capacity curves, which represent the envelop response of forces vs. displacements, i.e., the maximum measured reaction in the loading stage of each sequence. Under QS cyclic loading, these curves can be assimilated to the standard pushover curves, assuming that while compressed, the cracked concrete fully recovers its initial properties when the cracks have closed.
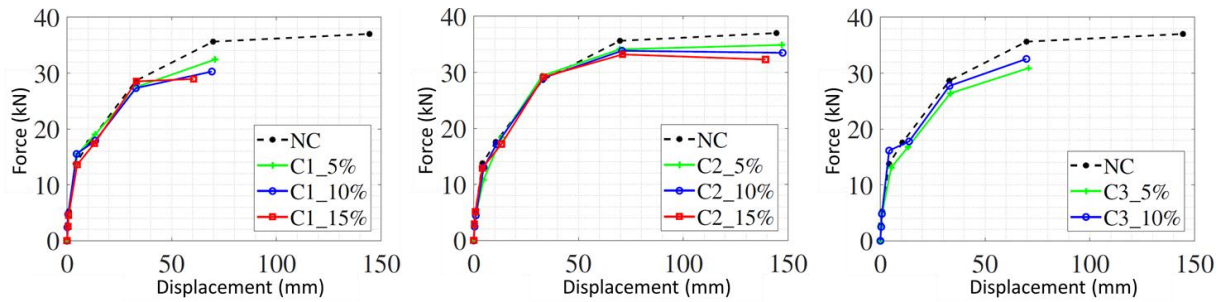
Figure 18. Capacity curves for all beam configurations under QS cyclic loading

From Figure 18, we see that C_1 and C_3 beams suffered a loss in bearing capacity and ductility. This behaviour was due to the reduction in the mechanical strength of the longitudinal steel rebar, which were strained in traction. The plastic plateau was also strongly reduced for these configurations. On the contrary, the reduction in bearing capacity and ductility was less important for C_2 beams: compared to the NC beam, the variation was limited to 12% for bearing capacity and 4% for ductility, which is due to the fact that the wrapping steel grid stiffness has no bending contribution.

The maximum ductility coefficient μ for each beam was quantified using the following equation:

$$\mu = \frac{\max_t |u(t)|}{u_y} \tag{1}$$

Where $u(t)$ is the displacement time history measured at beam mid-span. u_y is the mid-span displacement corresponding to the rebar plastic yielding for the studied beam, and obtained using Park's method (Park, 1989).

The characteristic values of displacements obtained for the QS tests are given in Table 2. From this table, we observe that u_y was almost constant for all tested beams, while the maximum displacement measured at mid-span decreased with the corrosion rate increase for C_1 and C_3 configurations. For C_2 beams, displacement values were similar to those obtained for the NC reference. As u_y remained almost constant for all tested beams, in the rest of the works, u_y was kept constant and equal to the yielding displacement of the NC beam.

Table 2: Displacements obtained by Park's method for all beam configurations under QS cyclic loading.

Beam configuration	u_y (mm)	$\max_t |u(t)|$ (mm)
NC	20.7	145.7
C_1 **5%**	22.3	72.2
C_1 **10%**	19.8	70.6
C_1 **15%**	21.2	33.5
C_2 **5%**	24.2	149.4
C_2 **10%**	21.7	150.3
C_2 **15%**	21.4	160.9
C_3 **5%**	19.4	72.1
C_3 **10%**	20	71.1

Figure 19 shows the evolution of μ in function of the corrosion rate. We see that the results are coherent with those obtained from the capacity curves of Figure 18.
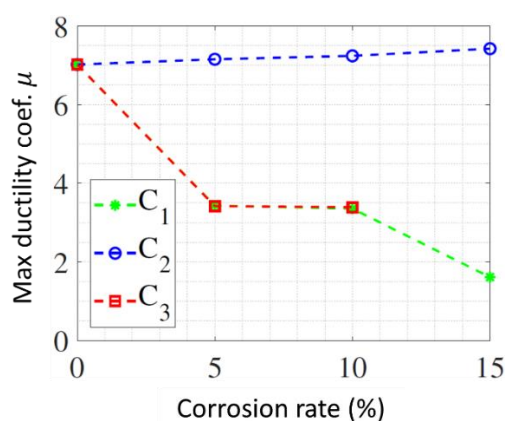
Figure 19. Evolution of maximum ductility coefficient µ for the various corrosion rates (QS cyclic loading)

3.6.2 *Main results for the dynamic tests*

The capacity curves are shown on Figure 20. Similarly to the QS tests, the C_1 and C_3 beams suffered a loss in maximum bearing capacity and ductility, while the C_2 beams displayed capacity curves very close to the NC beam one.
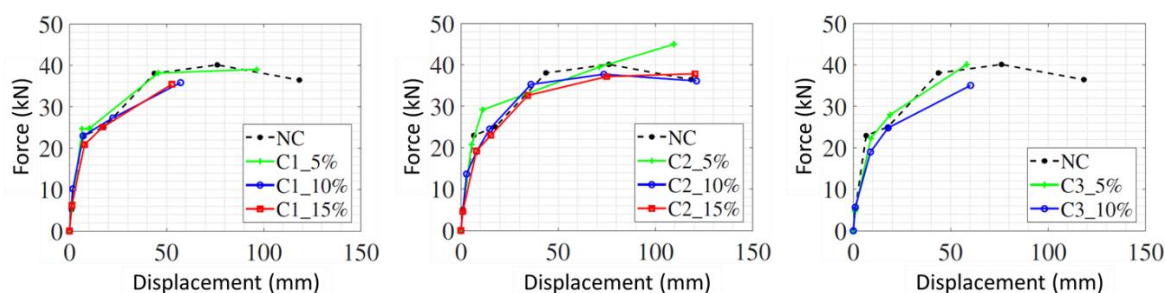
Figure 20. Capacity curves for all beam configurations under DYN loading

Contrary to the QS tests, some beams did not reach total failure, which made the quantification of the ductility coefficient μ more difficult, as the maximum displacement could not be measured for all the tested beams. Hence, it was decided to consider a PGA of 2.5 g for the excitation imposed to the shaking table, as it was common to all the non-failed beams. Then, the equation (1) was used to obtain μ with Park's method. The characteristic values of displacements obtained for the DYN tests are given in Table 3.

From this table, we see that both u_y and the maximum displacement values decreased drastically with the corrosion rate increase for C_1 configuration, while u_y values for the other configurations remained close to the NC one. Hence, to remain representative, the ductility coefficient μ for all corroded beams were computed by considering the u_y value for the NC beam. This method was used all along the next sections.

Table 3: Displacements obtained by Park's method for all beam configurations under DYN loading.

Beam configuration	u_y (mm)	$\max_t \lvert u(t) \rvert$ (mm)
NC	26.1	94
C_1 **5%**	15.5	65.4
C_1 **10%**	11	44
C_1 **15%**	17.1	52.7
C_2 **5%**	34.9	109.5
C_2 **10%**	20.7	121.2
C_2 **15%**	24.3	87.2
C_3 **5%**	27.1	58.3
C_3 **10%**	25.3	69.9

Figure 21 shows the evolution of μ in function of the corrosion rate. A decrease of the ductility coefficient with the corrosion rate was observed for C_1 and C_3 beams, while the one for C_2 configuration was close to the NC beam one.
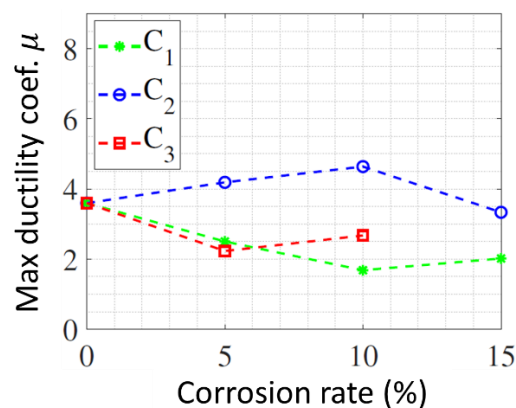
Figure 21. Evolution of maximum ductility coefficient μ for the various corrosion rates (DYN loading)

3.7   Analysis of the modal properties

3.7.1   Main results for the QS cyclic tests

A modal analysis was performed for each beam along the QS tests, using a hammer shock, hence allowing to quantify the evolution of the first eigenmode with respect to the ductility coefficient taken as main damage indicator.

Two methods were used to characterize the eigenmodes and associated damping:

  (1) the -3dB bandwidth method, which is usually applied for moderately damped systems with quite distinct eigenmodes (Chopra, 2012);
  (2) the stochastic subspace identification method (e.g., Lardies & Larbi, 2001; Li et al., 2019).

Figure 22 shows the evolution of the first eigenmode obtained with the stochastic subspace method. Results with the standard method were very close.
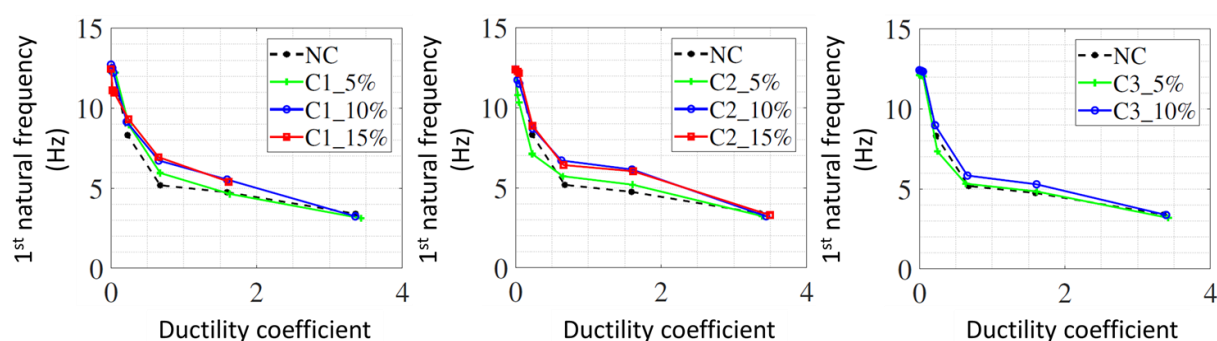
Figure 22. Identification of the evolution of the 1st mode obtained with the hammer shock, for all beam configurations, using the stochastic subspace method (QS cyclic loading)

A decrease in the 1st mode was observed for all configurations. Former studies (Maalej et al., 2010) have shown that this progressive decrease of the resonant mode is linked to the occurrence of cracking in the concrete, which results in a gradual loss of bending stiffness.

However, we observed that this trend was more important for the NC beam, although the corroded beams were more damaged. A possible explanation given by some authors (e.g., Maalej et al., 2010) is that the accelerated corrosion process where the continuous hydration of the concrete improves it mechanical features. A second reason may be that the steel-concrete bond is improved, leading to a higher natural frequency during the mechanical loading, until total failure (e.g., Amleh and Mirza, 1999). This second aspect was effectively observed during the DYSBAC campaign, for the corroded test samples.

It is also important to note that the modal identification means is important for the result interpretation. For instance, the natural frequency derived from hammer shock tests may be over-estimated, even for a NC beam. This is due to the local nature of the hammer shock excitation, which is not able to mobilize the overall structural nonlinearity. Hence, it was interesting within the DYSBAC campaign, to use different testing methods (e.g., white noise dynamic testing).

Figure 23 shows the evolution of the modal damping of the first eigenmode, obtained with the hammer shock, using the stochastic subspace method.
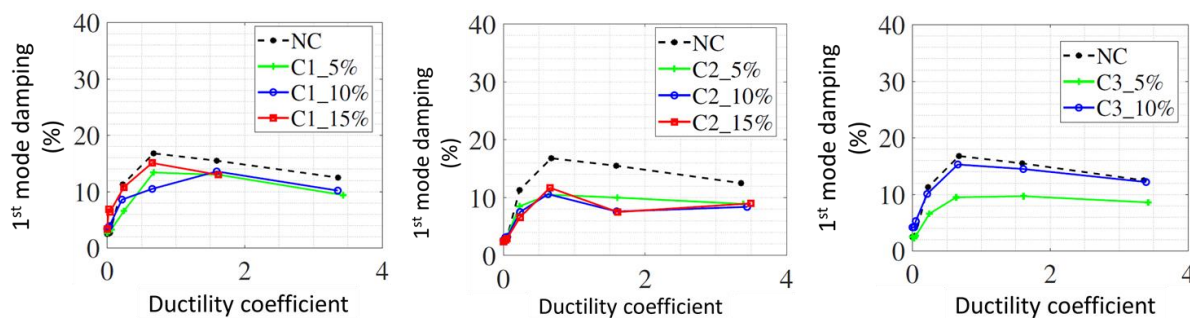
Figure 23. Identification of the evolution of the modal damping obtained with hammer shock, for the 1ˢᵗ mode and all beam configurations, using the stochastic subspace method (QS cyclic loading)

Contrary to the results related to the modal evolution, those related to the damping evolution in function of corrosion obtained with both identification methods were rather different, as shown in Table 4. This was due to the fact that the stochastic method was based on all available accelerometer measures, whereas the bandwidth one used only some of them.

No clear conclusion could be drawn from the bandwidth identification method, regarding the damping evolution in function of the corrosion rate, contrary to the stochastic subspace method, where the damping increase trend was stronger, especially for C_1 beams. This increase can be linked to the localized cracking in the concrete, which may lead to higher energy dissipation, as observed also in other experimental studies (e.g., Yuan et al., 2018).

As for the damping evolution in function of the ductility, both methods gave very similar results: damping tends to increase with damage (cracking in concrete) and then remains almost constant (rebar yielding).

Table 4: Modal damping ratios obtained for all beams, using the hammer shock before applying the QS cyclic loading.

Beam configuration	Modal Damping (%)	
	-3dB bandwidth method	Stochastic subspace method
NC	4	2.5
C_1 **5%**	3.6	2.7
C_1 **10%**	4.4	3.4
C_1 **15%**	4.5	3.4
C_2 **5%**	3.5	2.7
C_2 **10%**	3.3	2.6
C_2 **15%**	3.3	2.4
C_3 **5%**	3.6	2.5
C_3 **10%**	3.3	4.2

3.7.2   *Main results for the dynamic tests*

The modal analysis was performed by applying a white noise to each tested beam and using the same methods for modal identification.

Figure 24 shows the evolution of the first eigenmode obtained with the stochastic subspace method. Results with the standard method were very close.

We obtained similar conclusions as for the QS tests. One is that the 1ˢᵗ eigenmode cannot be considered as a relevant damage indicator for some cases (e.g., for beams with a low corrosion rate), since there is a strong dependency between the observed natural frequency, the damage location and the nature of the excitation used for modal identification (Salawu, 1997).
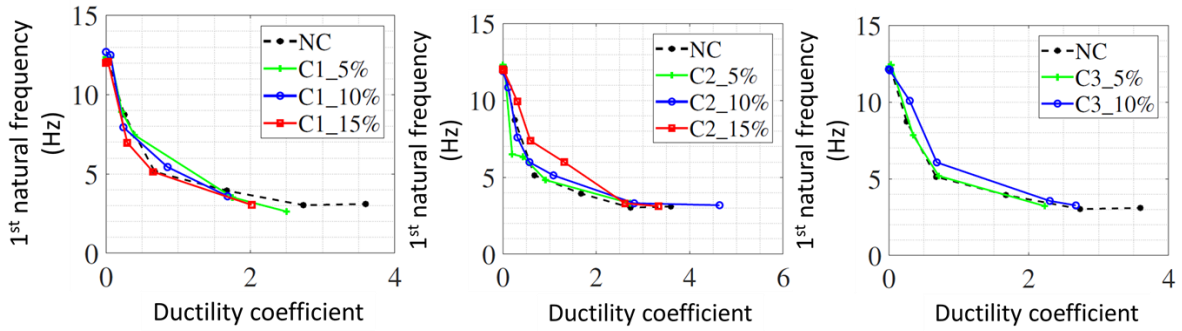
Figure 24. Identification of the evolution of the 1st mode obtained with a white noise, for all beam configurations, using the stochastic subspace method (DYN loading)

Figure 25 shows the evolution of the modal damping of the 1st eigenmode, obtained with the stochastic subspace method. Table 5 gives the damping ratios associated to the 1st eigenmode for both identification methods, and determined with a white noise applied to the beams before the seismic loading sequences. We obtained similar conclusions as for the QS tests: the increase in the modal damping coefficient in the case of corroded beams is linked to the corrosion effect.
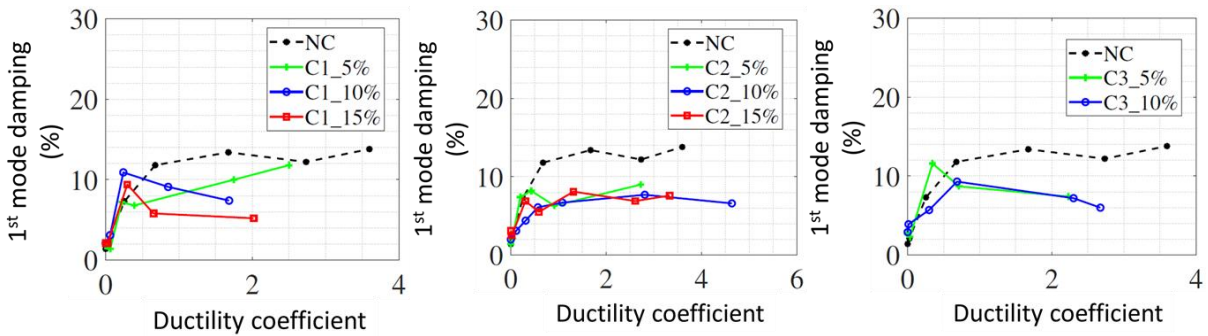
Figure 25. Identification of the evolution of the modal damping obtained with a white noise, for the 1st mode and all beam configurations, using the stochastic subspace method (DYN loading)

Table 5: Modal damping ratios obtained for all beams, using a white noise before applying the DYN loading.

Beam configuration	Modal Damping (%)	
	-3dB bandwidth method	Stochastic subspace method
NC	1.4	1.4
C_1 5%	2.5	1.8
C_1 10%	2.7	2.1
C_1 15%	1.8	2.1
C_2 5%	3.2	1.4
C_2 10%	4.1	2
C_2 15%	4.9	3.1
C_3 5%	3.2	2.8
C_3 10%	1.9	2.9

Similar damping values were observed for both identification methods, except for C_2 configuration, where the bandwidth method seemed to be overestimating. As noted for the hammer shock tests in the QS results, this may be due to the limited number of accelerometers used for this identification method. Hence, the stochastic subspace method should be preferred for modal identification of structures with a distributed damage, which may be the case for corroded elements.

3.8 Analysis of the energy dissipation

The modal damping ratios in the section 3.7, were obtained for all beams, by using low-level mechanical loadings (hammer shock, white noise). They cannot be used to assess the energy dissipation at higher levels, where material nonlinearity might be fully mobilized. Different strategies can be used to quantify the energy dissipation in this case.

3.8.1 Main results for the QS cyclic tests

The Equivalent Viscous Damping Ratio (EVDR or ξ_{eq}) can be used to assess the seismic behaviour of a RC structure, being an indicator of the structural capacity to dissipate the input energy. This parameter depends on the ductility level and on the plastic hinges location (Priestley, 1997), and can be obtained by summing the elastic and hysteretic damping values.

Following the Jacobsen's method for a single degree of freedom (SDOF) oscillator under a mono-harmonic loading (Jacobsen, 1960), ξ_{eq} can be derived as follows:

$$\xi_{eq} = \frac{1}{4\pi} \cdot \frac{\omega_0}{\omega} \cdot \frac{E_d}{E_s} \tag{2}$$

With:

      E_d Dissipated energy during one loading cycle (surface of the hysteretic loop)

      E_s Stored potential elastic energy

      ω Harmonic loading frequency

      ω_0 Natural frequency of the oscillator

In this study, we used an updated version of the Jacobsen's method, which is able to account for possible asymmetry in the hysteretic response (e.g., Heitz et al., 2019). The principle of the Jacobsen's method is illustrated on the Figure 26.
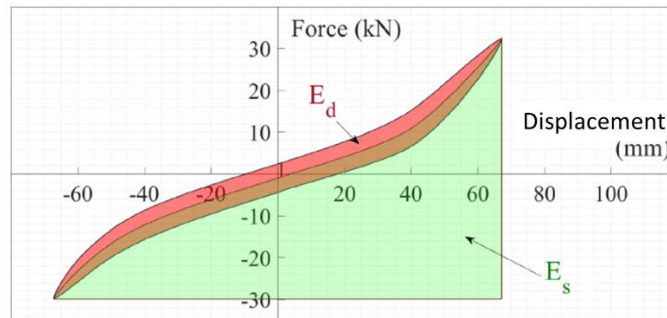
Figure 26. Principle of the Jacobsen's method

As shown on the Figure 27, the dissipated energy increased with respect to the mid-span displacement, for all tested beams, due to the damage increase (cracking in concrete). This was also observed in former studies (Panteliou et al., 2001). Moreover, dissipation capacity decreased with the corrosion rate increase, which is also coherent with former observations (Ma et al., 2012; Guo et al., 2015). Finally, no major difference could be observed between the different configurations at a same corrosion level.
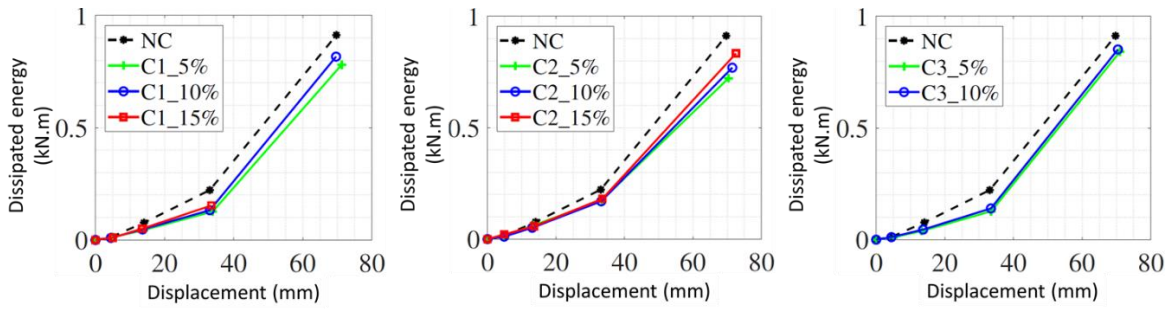
Figure 27. Evolution of the energy dissipation for all tested beams (QS cyclic tests)

As shown on the Figure 28, no major difference in the stored elastic energy with respect to the mid-span displacement, could be observed between the various beams tested. This result was not observed in the study by Guo et al. (2015) on bridge piers, where the stored energy was decreasing when the corrosion rate was increasing. This can be perfectly explained by the important differences between both studies, regarding the computing method, as well as the boundary and loading conditions.
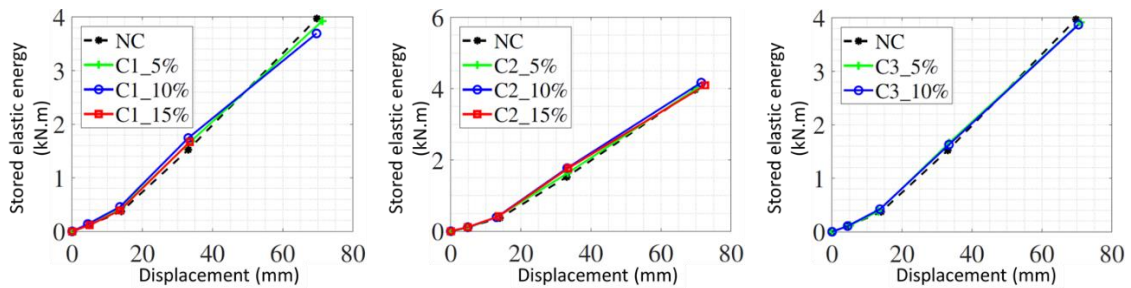
Figure 28. Evolution of the stored elastic energy for all tested beams (QS cyclic tests)

Finally, when plotting the estimated EVDR as a function of the mid-span displacement (Figure 29), we see that it is decreasing for the corroded beams, when compared to the NC one. This result was also observed by Ma et al. (2012).
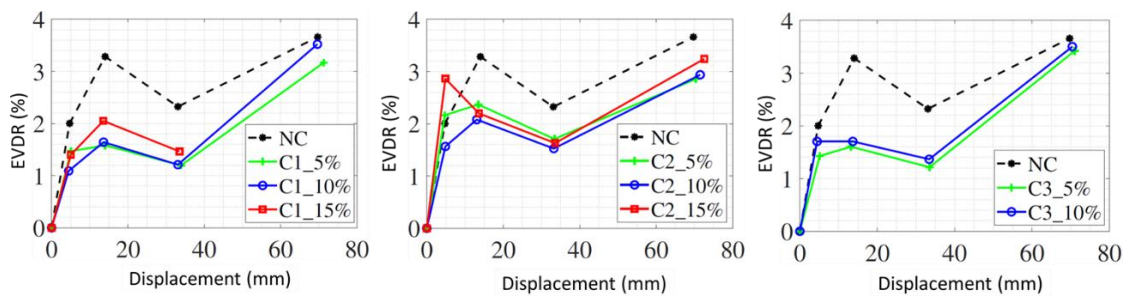
Figure 29. Evolution of the EVDR for all tested beams (QS cyclic tests)

3.8.2 Main results for the dynamic tests

Regarding the modal identification for high seismic loadings, two different methods were adopted in this work.

The first method was based on a time-frequency analysis, where the Fourier transform of the measured mid-span acceleration was calculated for each input seismic signal, using a sliding time-window and considering only the strong part of each seismic response (about 10 sec

duration). Then, as the seismic tests had different acceleration levels, each time-frequency diagram was normalized with respect to the maximum amplitude of the Fourier transform.

The resulting evolution of the modal response of all tested beams and for all seismic sequences, is shown on the Figure 30. Contrary to the results obtained with a white noise (low-level excitation), a drop in the natural frequency of the corroded beams was observed for all loading levels, which is explained by a the activation of all damage mechanisms when a realistic seismic loading is applied.
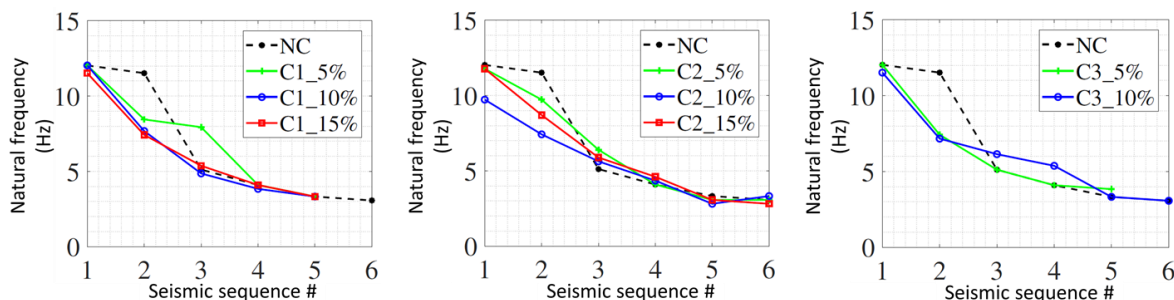
Figure 30. Evolution of the modal response for all tested beams (DYN tests)

The second method used in this work, allows to calculate the evolution of the modal damping ratio during the seismic loading, with no need to assume an evolution model for modal properties. Indeed, it is based on a non-parametric identification, which relies on the displacement fields measured through an image correlation technique (e.g., see details in Heitz et al., 2018).

This non-parametric identification method was used for each tested beam, in order to estimate the time evolution of the mean damping ratio for the 1st mode in function of the measured mid-span displacement, considering 4 acceleration levels: 0.125 g, 0.5 g, 0.8 g and 1.25 g.

From Figure 31, we observe that from the 2nd acceleration level on (2nd point on the curves), the mean damping estimated with this method for all tested beams, increases as the damage level increases. The high damping values were obtained at the last acceleration level (0.125 g) due to a poorer accuracy of the displacement field acquisition at this level.
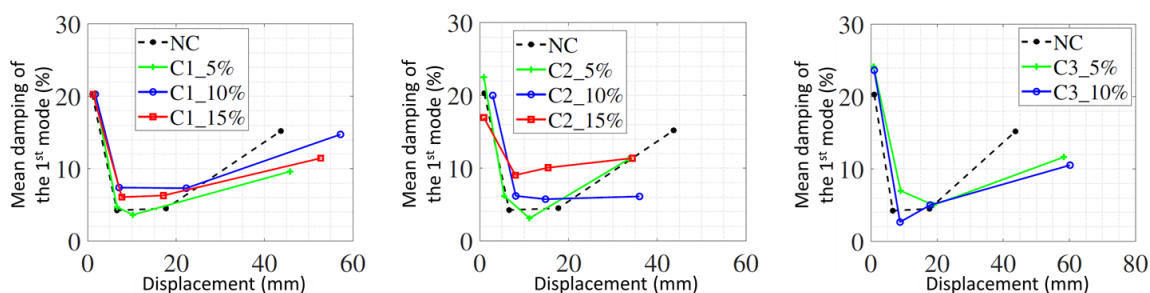
Figure 31. Evolution of the mean damping ratio for the 1st mode, obtained for all tested beams with the non-parametric identification method (DYN tests)

No clear trend between the effect of rebar corrosion and the modal damping evolution could be observed with this identification method. This is probably due to the choice of the mean value as representative parameter for the time evolution, as it hides the local variability, which is predominant in this case. However, thanks to this method, it is possible to evaluate the evolution of the natural frequencies and modal damping during the seismic loading. This is a key feature, as the modal properties of corroded structures vary significantly during seismic loadings.

4 Modelling strategy related to corrosion effects in reinforced-concrete structural members

4.1 Introduction

The experimental DYSBAC campaign detailed in the previous sections, has allowed to evaluate the influence of corrosion on some quantities of interest (QoI). However, in the frame of diagnosis and/or repair of existing corroded civil engineering structures, there is a need for numerical models able to predict the structural behaviour in case of external static or dynamic loadings.

The numerical model developed here and based on a finite-element formulation, is very well fitted for weakly corroded elements (3 to 9% of mass loss). It assumes the initial structural state is already corroded, and aims at modelling the effects of this corrosion on the material response. The proposed model can account for the following features:

- **Random distribution of corrosion pits**: Indeed, computations on corroded elements usually assume a uniform section reduction. In DYSBAC, we have shown that the beam failure did not systematically occur at mid-span, but it was rather depending on the stress distribution due to the corrosion pits.
- **Cracking in the concrete**: As shown in the previous sections, the initial measured damping ratio grows with the cracking in concrete. This deterioration in the quality of the cover concrete is usually modelled by means of a reduction in the compressive strength of the concrete. However, this modelling approach is not able to account for the effects of cracking on the energy dissipation.
- **Degradation of the mechanical behavior of steel**: It is usually modelled by the steel constitutive model (Ouglova, 2004).

In addition, the modelling strategy being based on Timoshenko fibre beam elements (Pegon, 1994; Guedes et al., 1994), it makes it easy to use at the structural scale and within a probabilistic safety assessment (PSA) framework, having a **low computing demand**.

In the following sections, we give an overview of the main features of the modelling strategy. More details can be found in the original PhD manuscript and related papers (Lejouad, 2020; Lejouad et al., 2019a,b; Lejouad et al., 2022a,b).

4.2 Modelling of the damage field in concrete due to the rebar swelling

Steel corrosion of the rebars leads to a swelling, which induces cracking in the concrete. In the model developed within the framework of this thesis, the representation of the damage variable at the concrete cross-section level has been preferred, as it allows to account for: (i) swelling and crack propagation in a realistic manner; (ii) concrete stiffness reduction due to cracking and hence leading to a better description of the elastic behaviour in case of corrosion.

A two-step modelling strategy has been developed and is described in the next sections.

4.2.1 Modelling the damaged concrete on a cross-section fine mesh

The steel volume increase due to corrosion is represented by an expansion factor α, expressed as follows:

$$\alpha = \frac{V_{cp}}{V_s} \tag{3}$$

With V_{cp}, the volume of the corrosion products and V_s, the corresponding volume of steel.

If we define the corrosion rate τ, as the steel mass loss relative to the initial steel mass, or equivalently, the ratio between the volume of the corrosion products on the rebar and the initial volume of the uncorroded rebar, then the rebar expansion Δr can be computed as:

$$\Delta r = r_c - r_i = \left(\sqrt{(\alpha - 1)\tau + 1} - 1\right) r_i \tag{4}$$

With r_c, the final radius of the corroded rebar and r_i, the initial radius of the rebar.

The concrete cross-section is modelled as a 2D domain, with a fine mesh, to accurately represent the damage field in the cross-section. The interface between steel and concrete is modelled using joint elements (e.g., Richard et al., 2010). The spatial variability of concrete is also taken into account through a random distribution of the Young modulus. Finally, concrete is modelled by the Mazars damage model (Mazars, 1986), where the stress tensor $\boldsymbol{\sigma}$ is expressed as follows:

$$\boldsymbol{\sigma} = (1 - D)\boldsymbol{K_0} : \boldsymbol{\varepsilon} \tag{5}$$

With D, the damage variable varying between 0 (no damage) and 1 (extensive damage); $\boldsymbol{K_0}$, the undamaged stiffness and $\boldsymbol{\varepsilon}$, the strain tensor.

Δr in eq. (4) will then be used to numerically compute the concrete damage due to the expansion of the corroded rebar. This latter is represented by a thermal expansion model, with a dilatation coefficient calibrated to match Δr.

4.2.2   *Transferring the damage field on a coarse cross-section mesh*

The damage distribution computed on each cross-section fine mesh, will then be used as the initial state for concrete to compute the whole beam response under seismic loading.

However, the use of such a fine mesh to discretize the fibre beam element cross-section, which is to be integrated into the whole beam computation, would mean to increase computation times drastically. Hence, the adopted strategy has been to project the computed damage field onto a coarser cross-section mesh, which will be the final fibre beam element cross-section for the seismic simulations.

Two projection methods to compute the initial damage field on the coarser cross-section mesh have been investigated in this work:

- A first method based on the use of the shape functions, as illustrated in Figure 32;
- A second method based on Moving Least Squares (MLS), e.g., as proposed by Brancherie et al., 2008.
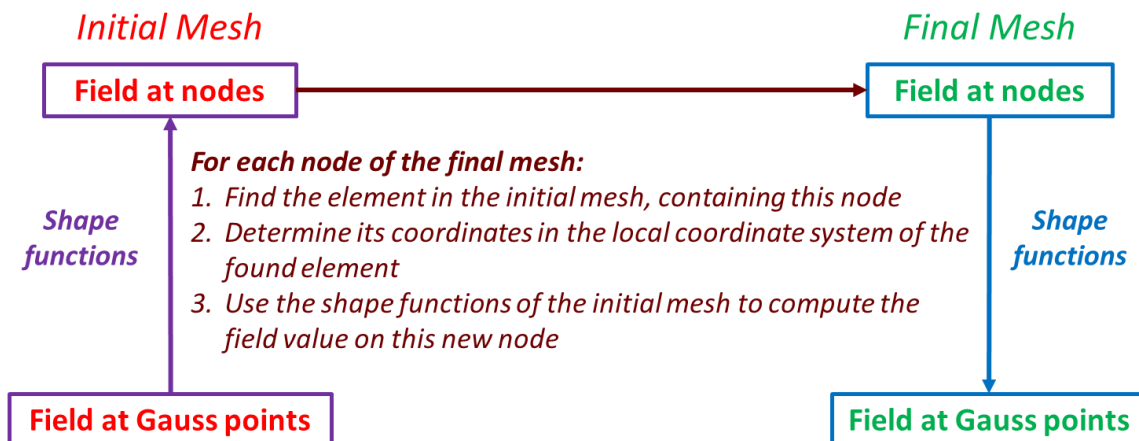
Figure 32. Method to transfer some computed fields between two meshes, using the shape functions

As the projection modifies the cross-section stiffness matrix, an optimization procedure has been proposed and used with both projection methods, to minimize the difference between the stiffness matrices for the fine and coarser cross-section meshes. The damage field resulting from the transfer from the cross-section fine mesh to coarser meshes is shown on Figure 33 for the optimised shape function method and on Figure 34, for the optimised MLS method. This last method presents a more diffuse damage profile: this is due to the number of neighbouring points considered, which strongly depends on the mesh shape.
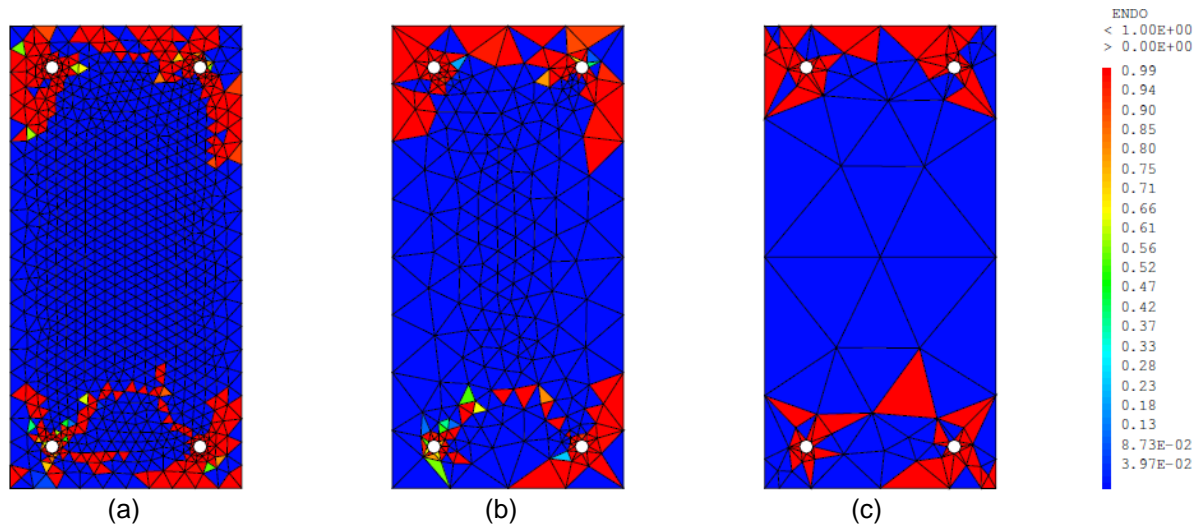
Figure 33. Damage field transferred with the optimised shape function method, for various meshes: (a) 1,686 elements (fine); (b) 452 and (c) 156 elements (coarse)
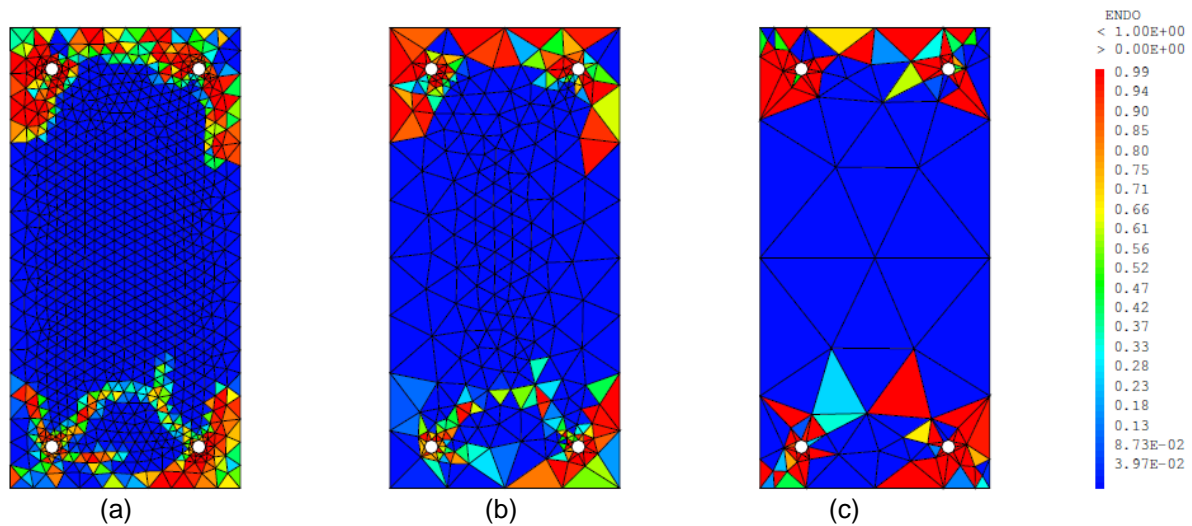
Figure 34. Damage field transferred with the optimised MLS method, for various meshes: (a) 1,686 elements (fine); (b) 452 and (c) 156 elements (coarse)

Finally, once a suitable projection of the damage field has been performed, the final damaged cross-section (coarse mesh) can be included in a fibre beam element. The damaged state of the material is taken as initial state, before applying the seismic loading.

4.2.3 *Modelling of the random distribution of corrosion pits*

As observed in the section 3, there exists a strong dependency between the spatial distribution of the corrosion pits and the failure location, even for low corrosion rates. Hence, a strategy to model the distribution of corrosion pits has been developed in this work, based on the experimental data. Indeed, the diameters along the corroded rebars have been measured every 1 mm, using a dedicated profilometric bench developed as part of the thesis work, and equipped with an on-board laser scanning sensor.

Many previous studies have shown that the occurrence of corrosion pitting is a random process (e.g., Stewart, 2004) or variable (Hawn, 1977). In this work, we have first characterised the auto-correlation for the series of measures available for the different corrosion rates (0, 5, 10 and 15%).

This auto-correlation analysis has revealed a number of interesting trends:

- The diameter distributions corresponding to the non-corroded (NC) rebar and the rebar corroded at 5% present a certain periodicity.
- Regarding the diameter distributions for the rebars with 10% and 15% corrosion rates, the periodicity seems no longer prevailing. This observed trend is considered indicative of a series that tends to increase or decrease linearly or exponentially in space (Venables and Ripley, 2002).

Then, the empirical cumulative distribution (cdf) and the probability density (pdf) functions have been derived from the diameter measures on the corroded rebars. As shown on the Figure 35, the shape of the distribution functions are similar for the NC and 5% corrosion rebars. We see also that the more the bar is corroded, the greater the probability of obtaining small diameters.
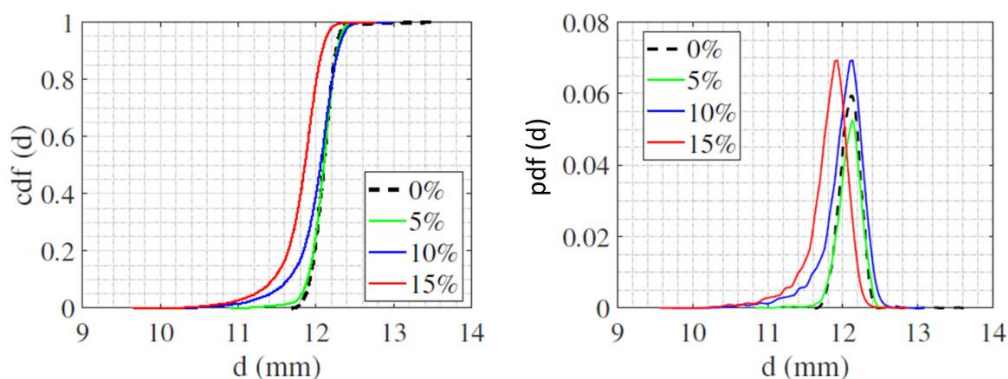
Figure 35. Statistical functions derived from the diameter measures on the rebars for the different corrosion rates

From the obtained distribution functions, it is possible to generate a sample composed of *m* diameter measurements characterized by the same distribution function, which can be used in the numerical model.

In our work, we have used the Karhunen–Loeve (Newman, 1996a,b) method which is based on a modal decomposition approach and significantly reduces the computation times. With this method, hundreds of distributions could be generated, which can be useful then for probabilistic mechanical analyses.

4.2.4 *Modelling of the corroded RC beam response to a seismic loading*

Figure 36 shows the beam longitudinal modelling principle, where blue nodes either represent sensors or beam supports.

The additional masses (360 kg) used for the experimental setting, have been affected on nodes P1L et P1R. The gravity centre of these masses being close to the beam neutral fibre, the rotational inertia have not been taken into account in the simulations.
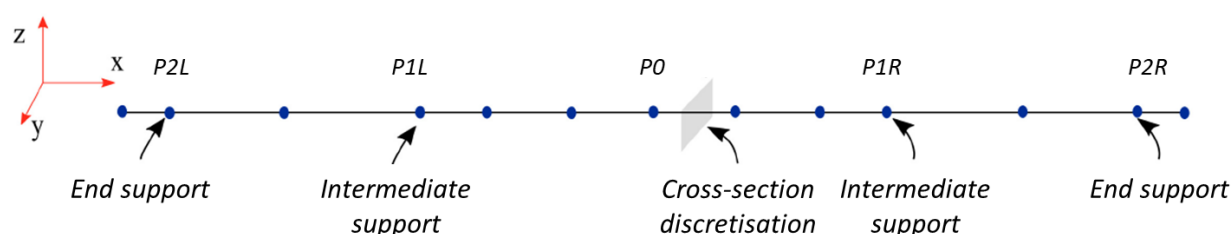
Figure 36. Longitudinal finite-element modelling principle for the whole beam

Figure 37 illustrates the final mesh containing 12 fibre beam elements distributed along the beam and a detailed view of the final cross-section (coarse) mesh. In this latter, each steel rebar has been modelled as a "point element" affected by its section and moment of inertia properties, and located at the center of the rebar section. Due to the fibre beam element formulation, the bond between steel and concrete has been considered perfect in the numerical simulations.
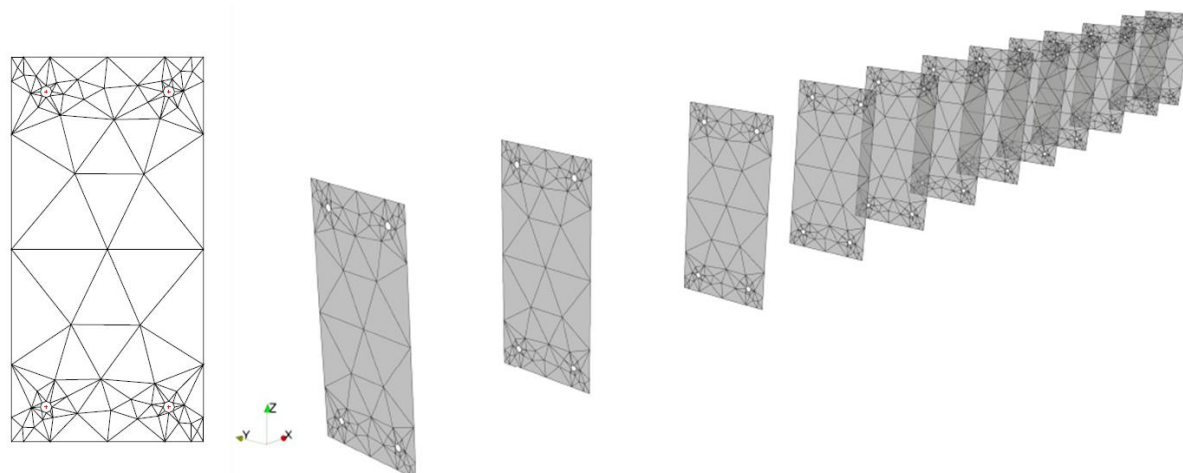
Figure 37. Coarse cross-section mesh (left) and fibre beam elements for the DYSBAC beam (right)

Regarding the boundary conditions on nodes *P2L* and *P2R* in Figure 36, all degrees of freedom have been blocked, except the rotations around z axis (both nodes), and the translations along x-axis (*P2R* only).

Regarding the whole beam simulations, the constitutive models of Ouglova (Ouglova, 2004) and RICBET_UNI (Richard and Ragueneau, 2013), have been used respectively for the steel and the concrete elements. Indeed, although being robust for monotonous loadings, the Mazars damage model (Mazars, 1986) cannot be used in case of cyclic loadings on brittle materials, as it cannot account for the crack reclosing. However, the damage computations due to the rebar swelling have been performed with the Mazars model, as in the finite-element computation code we use (CASTEM, e.g., see Millard, 1993), the RICBET_UNI model is not implemented for the plane strains formulation.

Finally, the loading sequences used during the experimental tests have been imposed the beam. Regarding the dynamic test simulations, an additional viscous damping (Rayleigh) of 2% has been considered.

The overall modelling strategy to account for corrosion effects in the seismic response of corroded reinforced-concrete beams is summarised in the Figure 38. It has been applied to the C_1 beams, for various target corrosion rates {0%; 5%; 10%; 15%}, corresponding to the effective (measured) corrosion rates {0%; 3.1%; 6.3%; 9.4%}.

A comparison between the experimental and numerical results for the different simulated beams has been performed, in terms of the QS cyclic (force-displacement curve) and dynamic (acceleration) responses. The sensitivity of the structural responses to the various aspects (cracking of the concrete, steel constitutive behaviour, non-uniform diameter distribution along the steel rebars) has been evaluated. A single diameter distribution has been assumed for all rebars of a given corrosion rate.
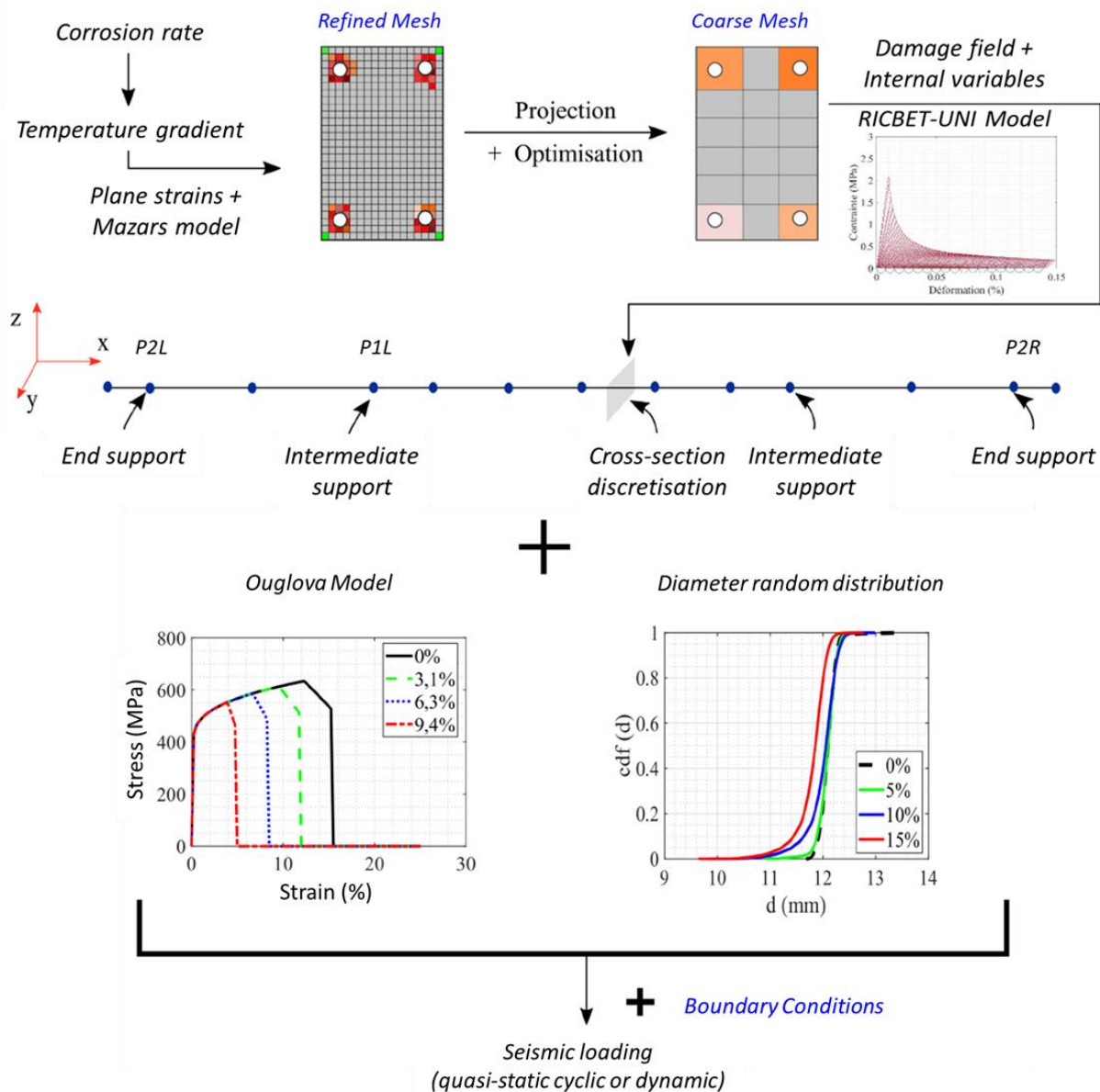
Figure 38. Modelling strategy to account for corrosion effects in the seismic response of corroded RC beams

Three levels of loading have been considered in simulations:

- The **low loading level** corresponds to the 1st imposed displacement (±0.8 mm) in the QS case, and to the 1st applied seismic signal (0.125 g) in the DYN case.
- The **intermediate loading level** corresponds to an imposed displacement of ±25 mm in the QS case, and to an applied seismic signal of 0.5 g in the DYN case.
- The **high loading level** corresponds to the last imposed displacement in the QS case (leading to failure), and to the last applied seismic signal in the DYN case.

With the fibre beam element formulation, the failure (QS case) occurs when at least one steel fibre in at least one cross-section (fibre element) has exceeded the ultimate strain, which introduces a divergence at the end of the iterations within the concerned time step. This is depicted by some outliers in the associated force-displacement curves.

In Figure 39, Figure 40 and Figure 41, we show an example of the comparison between the experimental and numerical results obtained for the 10% (effective 6.3%) corrosion rate. The Table 6 gives the meaning of the legends used in the figures.

Table 6: Figure legend used to compare the experimental and numerical results.

Figure legend	Meaning
EXP	Experimental response
SU	Simulation accounting for the steel behaviour degradation + a uniform section (diameter random distribution not considered)
NU	Simulation accounting for the steel behaviour degradation + a non-uniform section (diameter random distribution considered)
ENDO_SU	Simulation combining the damage of concrete and SU configuration
ENDO_NU	Simulation combining the damage of concrete and NU configuration

From the results obtained for C_1 beams and the three corrosion rates, several lessons could be drawn:

- The expansion coefficient as well as the average corrosion rate to be considered determine the computed damage state, but both quantities nevertheless remain difficult to calibrate.
- Accounting for the damage does not significantly improve the results of the model at the various levels of loading. This conclusion is valid for the relatively low corrosion rates (3% to 10%) targeted by the DYSBAC experimental campaign. However, this aspect can be of great importance in the case of heavily corroded structural elements.
- Accounting for the diameter distribution is an important factor, to be able to predict the rupture of the test body, unlike the assumption of a uniform section.

It is important to emphasize that all the numerical simulations have been carried out by considering a single diameter distribution per corrosion rate. However, the random nature of the corrosion pathology would require to perform several simulations with several diameter distributions.

(a)   (b)   (c)
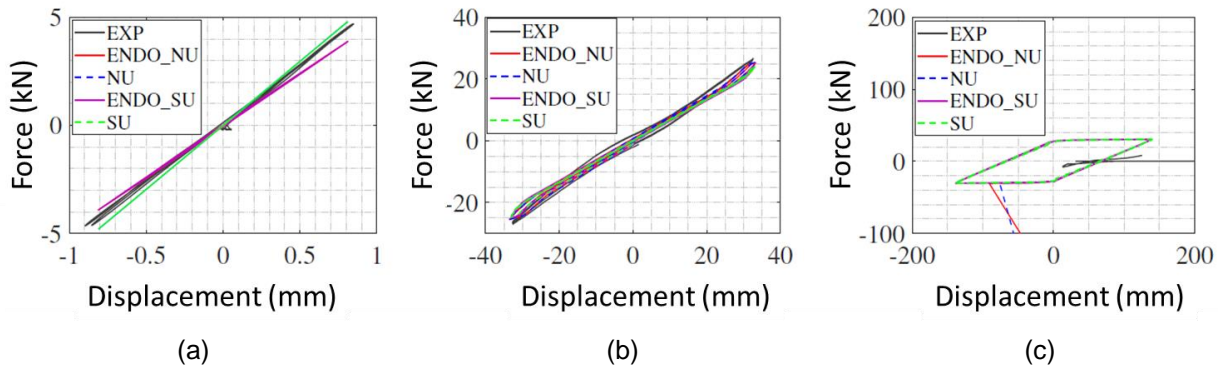
Figure 39. QS responses for the C_1 beam with 10% corrosion rate for low (a), intermediate (b) and high (c) loading levels

(a)   (b)   (c)
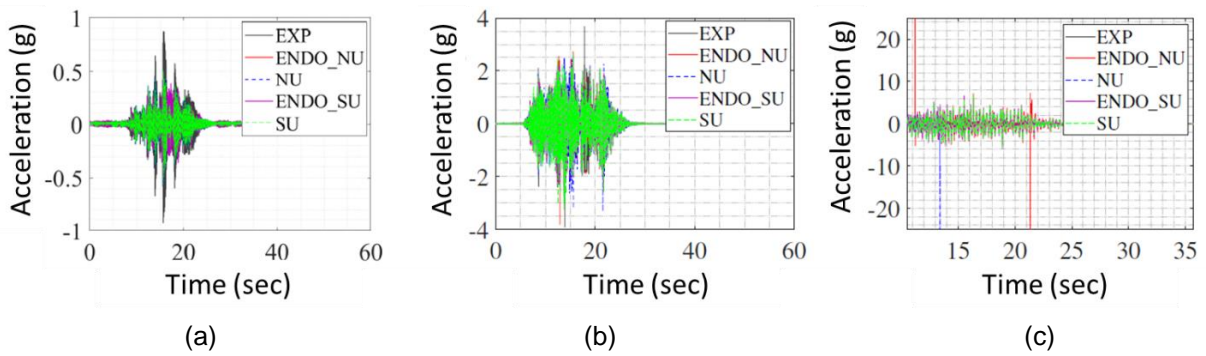
Figure 40. DYN responses (acceleration) for the C_1 beam with 10% corrosion rate for low (a), intermediate (b) and high (c) loading levels

(a)   (b)   (c)
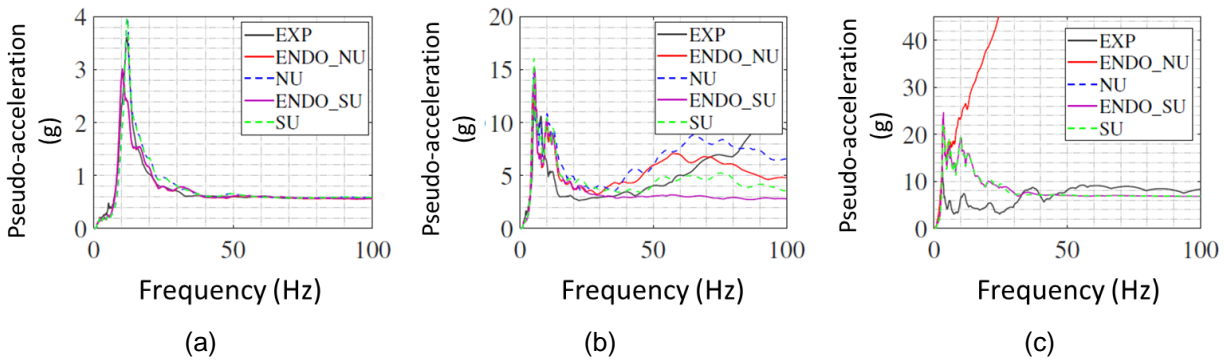
Figure 41. DYN responses (spectral acceleration) for the C_1 beam with 10% corrosion rate for low (a), intermediate (b) and high (c) loading levels

5   Conclusions

The bibliographic study carried out in this PhD works has reported a large number of studies allowing the characterization of the mechanical behaviour of corroded RC structural elements. However, it has revealed an important need in terms of experimental data acquisition on corroded structural elements under various loading (quasi-static cyclic, dynamic). Moreover, very few scientific contributions have addressed the dynamic loading. In addition, the numerical simulations carried out were focused on the consequences of the corrosion pathology at the material scale (cracking, steel/concrete bond and degradation of the steel constitutive behaviour). However, an aspect which is often neglected although crucial as it conditions the mechanical behaviour of corroded structures, is the formation of localized corrosion pits.

Our thesis work contributes to filling the aforementioned gaps through the DYSBAC experimental campaign carried out on large-scale RC beams corroded with an accelerated corrosion technique. Three corrosion configurations in the steel rebars (longitudinal, transverse and total) have been considered, in order to assess the influence of each configuration on the structural response. Two types of loading (quasi-static cyclic and dynamic) as well as of modal identification (hammer shock and white noise) have been applied to the test bodies, keeping the same experimental setup.

The results of the DYSBAC experimental campaign have highlighted different responses for the beams affected by corrosion in comparison with a healthy beam: greater in displacements and less significant in acceleration. In addition, a degradation of the bearing capacity, ductility and dissipation capacity with the development of corrosion pathology, especially for the longitudinal and total corrosion test bodies, has been observed. The modal identifications carried out on the tested beams, before applying any loading, have shown an increasing damping coefficient according to the degree of corrosion, contrary to the natural frequency for which no specific trend could be noted. The use of more test bodies would probably have made it possible to observe a specific trend. The modal properties measured between each successive loading have shown an increase in the natural frequency and a decrease in the damping coefficient as a function of the degree of corrosion at the same loading level, in particular for the beams in the transverse corrosion configuration. Quasi-static as well as dynamic tests have confirmed these trends.

The numerical model developed as part of this thesis work aims at predicting the quasi-static and dynamic response of weakly corroded structural elements (3% to 9% loss of mass) with reasonable computational costs. Therefore, the Timoshenko fibre beam elements formulation has been preferred. The model is able to account for the cracking of the concrete induced by the expansive nature of the corrosion products. This cracking state is first simulated on a fine mesh by applying a thermal loading on the joint elements representing the steel/concrete bond. The damage field obtained for this fine mesh is then projected on a coarser mesh in order to keep a low computing demand when using the fibre beam elements. Hence, a field projection method has been used, which allows to minimise the difference between the two cross-section (initial and projected) stiffness matrices. The steel mechanical degradation is then taken into account through the constitutive model while the spatial distribution function for the corrosion pits is determined from the experimental measures performed on the corroded rebars sections. The proposed numerical model is thus capable of predicting the beam failure in agreement with the experimental results. In addition, it has been shown that taking cracking into account improves the prediction of the structural responses at low loading levels for the most corroded beam. However, the determination of the expansion coefficient to be considered in the simulations remains a difficult task.

In conclusion, this work has improved the state of knowledge on the dynamic behaviour of weakly corroded structural elements (3% to 9% loss of mass), as well as on the most determining elements to be considered in the numerical simulations and models. The use of quasi-static cyclic tests in the prediction of seismic response of corroded structures is also relevant, as attested by the good agreement observed between the results of dynamic and

quasi-static tests. Moreover, the trends noted at the end of the modal characterizations show that the modal properties (natural frequency and damping) are not reliable indicators of damage. This is due not only to the intrinsic nature of the characterization test or the identification method used but above all to the combination of several mechanisms with contradictory effects on these modal properties: improvement in the quality of the concrete due to the continuous hydration of the concrete during the accelerated corrosion protocol; localized occurrence of micro-cracks; steel/concrete bond quality; non-uniform distribution of the corrosion pits...

With regard to the numerical aspects, the simulations carried out show that the non-uniform distribution of the steel rebar section as well as the degradation of the mechanical behaviour of the corroded steel are key elements to consider when predicting the response of corroded structures, in particular their failure.

References

Amleh, L. and Mirza, S. (1999). Corrosion influence on bond between steel and concrete. *Structural Journal*, **96**(3): 415-423.

Auyeung, Y., Balaguru, P., and Chung, L. (2000). Bond behavior of corroded reinforcement bars. *Materials Journal*, **97**(2): 214-220.

Brancherie, D., Villon, P., and Ibrahimbegovic, A. (2008). On a consistent field transfer in non linear inelastic analysis and ultimate load computation. *Comput. Mech.*, **42**(2): 213-226.

Chopra, A. K. (2012). Dynamics of structures. Pearson Education Upper Saddle River, NJ.

Cremona, C. Durée de vie des ouvrages : Approche prédictive, performantielle et probabiliste – Le Projet APPLET. Conference GC'2009, Paris, France, March 18-19, 2009.

Guedes, J., Pegon, P., and Pinto, A. V. (1994). A fibre Timoshenko beam element in CASTEM 2000. Special publication Nr. I, **94**: 55.

Guo, A., Li, H., Ba, X., Guan, X., and Li, H. (2015). Experimental investigation on the cyclic performance of reinforced concrete piers with chloride-induced corrosion in marine environment. *Engineering Structures*, **105**: 1-11.

Hawn, D. E. (1977). Extreme value prediction of maximum pits on pipelines. *Mater. Performance* (USA), **16**.

Heitz, T., Le Maoult, A., Richard, B., Giry, C., & Ragueneau, F. (2018). Dissipations in reinforced concrete components: Static and dynamic experimental identification strategy. *Engineering Structures*, **163**: 436-451.

Heitz, T., Giry, C., Richard, B., and Ragueneau, F. (2019). Identification of an equivalent viscous damping function depending on engineering demand parameters. *Engineering Structures*, **188**: 637-649.

Jacobsen, L. S. (1960). Damping in composite structures. *II WCEE*, Tokyo, 1960.

Lardies, J. and Larbi, N. (2001). Dynamic system parameter identification by stochastic realization methods. *Journal of Vibration and Control*, **7**(5): 711-728.

Lejouad, C. (2020). Compréhension du fonctionnement dynamique de structures en béton armé en présence de corrosion. *PhD Thesis*, Université Paris-Saclay (in French).

Lejouad, C., Capdevielle S., Richard, B., Ragueneau, F. (2019a). A numerical model to predict the effect of corrosion on the dynamic behavior of reinforced concrete beams.*12th Canadian Conf. on Earthq. Engng. (CCEE 2019)*, Québec, June 17-20.

Lejouad C., Richard B., Mongabure P., Capdevielle S., Ragueneau F. (2019b). Experimental Study Of The Seismic Behavior Of Corroded RC Beams. *SMIRT25*, Charlotte, USA. August 4-9, paper II_837. https://repository.lib.ncsu.edu/bitstream/handle/1840.20/37601/II_837_Chaymaa_Lejouad.pdf?sequence=1&isAllowed=y

Lejouad, C., Richard, B., Mongabure, P., Capdevielle S., Ragueneau, F. (2022a). Experimental study of corroded RC beams: dissipation and equivalent viscous damping ratio identification. *Materials and Structures*, **55**: 73. https://doi.org/10.1617/s11527-022-01906-y.

Lejouad, C., Richard, B., Mongabure, P., Capdevielle S., Ragueneau, F. (2022b). Assessment of the seismic behavior of reinforced concrete elements affected by corrosion: An objective comparison between quasi-static and dynamic tests. Structures **39:** 653-666. https://doi.org/10.1016/j.istruc.2022.03.058.

Li, Z., Fu, J., Liang, Q., Mao, H., and He, Y. (2019). Modal identification of civil structures via covariance-driven stochastic subspace method. *Math. Biosciences & Engng.*, **16**(5): 5709-5728.

Ma, Y., Che, Y., and Gong, J. (2012). Behavior of corrosion damaged circular reinforced concrete columns under cyclic loading. *Construction & Building Materials*, **29**: 548-556.

Maalej, M., Chhoa, C. Y., and Quek, S. T. (2010). Effect of cracking, corrosion and repair on the frequency response of RC beams. *Construction & Build. Materials*, **24**(5): 719-731.

Mazars, J. (1986). A description of micro-and macroscale damage of concrete structures. *Engineering Fracture Mechanics*, **25**(5-6): 729-737.

Meda, A., Mostosi, S., Rinaldi, Z., and Riva, P. (2014). Experimental evaluation of the corrosion influence on the cyclic behaviour of RC columns. *Engineering Structures*, **76**: 112-123.

Millard, A. (1993). Castem 2000 user manual. Technical report CEA-LAMBS (93/007).

Newman, A. J. (1996a). Model reduction via the Karhunen-Loeve expansion Part I: an exposition. Technical report.

Newman, A. J. (1996b). Model reduction via the Karhunen-Loeve expansion Part II: Some elementary examples. Technical report.

Ouglova, A. (2004). Etude du comportement mécanique des structures en béton armé atteintes par la corrosion. *PhD Thesis*, Ecole Normale Supérieure de Cachan (in French).

Panteliou, S. D., Chondros, T. G., Argyrakis, V. C., and Dimarogonas, A. D. (2001). Damping factor as an indicator of crack severity. *Journal of Sound and Vibration*, **241**(2): 235-245.

Park, R. (1989). Evaluation of ductility of structures and structural assemblages from laboratory testing. *Bull. New Zealand Soc. for Earthquake Engineering*, **22**(3): 155-166.

Pegon, P. (1994). A Timoshenko simple beam element in Castem 2000. *Technical Report, JRC, I-21020*, Ispra, Italy. Special publication Nr. I, **94**.

Priestley, M. J. N. (1997). Displacement-based seismic assessment of reinforced concrete buildings. *Journal of Earthquake Engineering*, **1**(01): 157-192.

Richard, B., Ragueneau, F., Cremona, C., Adelaide, L., and Tailhan, J. L. (2010). A three-dimensional steel/concrete interface model including corrosion effects. *Engineering Fracture Mechanics*, **77**(6): 951-973.

Salawu, O. S. (1997). Detection of structural damage through changes in frequency : a review. *Engineering structures*, **19**(9): 718-723.

Stewart, M. G. (2004). Spatial variability of pitting corrosion and its influence on structural fragility and reliability of RC beams in flexure. *Structural Safety*, **26**(4): 453-470.

Venables, W. N. and Ripley, B. D. (2002). Modern Applied Statistics with S. New York, Springer.

Yuan, W., Guo, A., Yuan, W., and Li, H. (2018). Shaking table tests of coastal bridge piers with different levels of corrosion damage caused by chloride penetration. *Construction and Building Materials*, **173**: 160-171.